University of Groningen

Characterization of immune checkpoint inhibitor-induced cardiotoxicity reveals interleukin-17A as a driver of cardiac dysfunction after anti-PD-1 treatment

Gergely, Tamás G.; Kucsera, Dániel; Tóth, Viktória E.; Kovács, Tamás; Sayour, Nabil V.; Drobni, Zsófia D.; Ruppert, Mihály; Petrovich, Balázs; Ágg, Bence; Onódi, Zsófia

IMPORTANT NOTE: You are advised to consult the publisher's version (publisher's PDF) if you wish to cite from it. Please check the document version below.

Document Version
Publisher's PDF, also known as Version of record

Publication date:
2023

[Link to publication in University of Groningen/UMCG research database](#)

RESEARCH ARTICLE

Characterization of immune checkpoint inhibitor-induced cardiotoxicity reveals interleukin-17A as a driver of cardiac dysfunction after anti-PD-1 treatment

Tamás G. Gergely[1,2,3] | Dániel Kucsera[1,2,3] | Viktória E. Tóth[1,2,3] |
Tamás Kovács[1,2,3] | Nabil V. Sayour[1,2,3] | Zsófia D. Drobni[4] | Mihály Ruppert[4] |
Balázs Petrovich[1] | Bence Ágg[1,5,6] | Zsófia Onódi[1,2,3] | Nóra Fekete[7] |
Éva Pállinger[7] | Edit I. Buzás[7] | Laura I. Yousif[8,9] | Wouter C. Meijers[8,9] |
Tamás Radovits[4] | Béla Merkely[4] | Péter Ferdinandy[1,5,6] | Zoltán V. Varga[1,2,3]

[1]Department of Pharmacology and Pharmacotherapy, Semmelweis University, Budapest, Hungary

[2]HCEMM-SE Cardiometabolic Immunology Research Group, Semmelweis University, Budapest, Hungary

[3]MTA-SE Momentum Cardio-Oncology and Cardioimmunology Research Group, Semmelweis University, Budapest, Hungary

[4]Heart and Vascular Center, Semmelweis University, Budapest, Hungary

[5]Pharmahungary Group, Szeged, Hungary

[6]MTA-SE System Pharmacology Research Group, Department of Pharmacology and Pharmacotherapy, Semmelweis University, Budapest, Hungary

[7]Department of Genetics, Cell- and Immunobiology, Semmelweis University, Budapest, Hungary

[8]Department of Cardiology, Medical Center Groningen, University of Groningen, Groningen, The Netherlands

[9]Division of Experimental Cardiology, Department of Cardiology, Thorax Center, Erasmus University Medical Center, Rotterdam, The Netherlands

Correspondence

Zoltán V. Varga, MTA-SE Momentum Cardio-Oncology and Cardioimmunology Research Group, Semmelweis University, Budapest, H-1089 Budapest, Nagyvárad tér 4, Hungary.
Email: varga.zoltan@med.semmelweis-univ.hu

Funding information

The work was supported by the European Union's Horizon 2020 Research and Innovation Programme under grant agreement no. 739593 and by a Momentum Research Grant from the Hungarian Academy of Sciences (LP-2021-14 to ZVV). Project no. RRF-2.3.1-21-2022-00003 has been implemented with the support provided by the European Union. NVKP_16-1-2016-0017 ("National Heart Program") has been implemented with the support provided from the National Research, Development and

Background and Purpose: Immune checkpoint inhibitors (ICI), such as anti-PD-1 monoclonal antibodies, have revolutionized cancer therapy by enhancing the cyto-toxic effects of T-cells against tumours. However, enhanced T-cell activity also may cause myocarditis and cardiotoxicity. Our understanding of the mechanisms of ICI-induced cardiotoxicity is limited. Here, we aimed to investigate the effect of PD-1 inhibition on cardiac function and explore the molecular mechanisms of ICI-induced cardiotoxicity.

Experimental Approach: C57BL6/J and BALB/c mice were treated with isotype control or anti-PD-1 antibody.

Echocardiography was used to assess cardiac function. Cardiac transcriptomic changes were investigated by bulk RNA sequencing. Inflammatory changes were assessed by qRT-PCR and immunohistochemistry in heart, thymus, and spleen of the

Abbreviations: Aif1, allograft inflammatory factor; Ass1, argininosuccinate synthase 1; CTLA-4, cytotoxic T-cell antigen-4; Fxyd2, FXYD domain containing ion transport regulator 2; Gata3, GATA binding protein 3; Gsk3b, glycogen synthase kinase 3 beta; Icam1, intercellular adhesion molecule 1; irAE, immune-related adverse events; Ldb3, LIM domain binding 3; LVEDV, left ventricular end-diastolic volume; LVESV, left ventricular end-systolic volume; LVIDd, left ventricular internal diameter in diastole; LVIDs, left ventricular internal diameter in systole; LVSD, left ventricular systolic dysfunction; Nfkbia, nuclear factor-kappa-B-inhibitor alpha; Ppia, peptidylprolyl isomerase A; Rora, RAR-related orphan receptor alpha; Rorc, RAR-related orphan receptor gamma; Rpl13a, ribosomal protein L13a; Stat3, signal transducer and activator of transcription 3; Tbx21, T-box transcription factor 21.

animals. In follow-up experiments, anti-CD4 and anti-IL-17A antibodies were used along with PD-1 blockade in C57BL/6J mice.

Key Results: Anti-PD-1 treatment led to cardiac dysfunction and left ventricular dilation in C57BL/6J mice, with increased nitrosative stress. Only mild inflammation was observed in the heart. However, PD-1 inhibition resulted in enhanced thymic inflammatory signalling, where *Il17a* increased most prominently. In BALB/c mice, cardiac dysfunction was not evident, and thymic inflammatory activation was more balanced. Inhibition of IL-17A prevented anti-PD-1-induced cardiac dysfunction in C57BL6/J mice. Comparing myocardial transcriptomic changes in C57BL/6J and BALB/c mice, differentially regulated genes (*Dmd*, *Ass1*, *Chrm2*, *Nfkbia*, *Stat3*, *Gsk3b*, *Cxcl9*, *Fxyd2*, and *Ldb3*) were revealed, related to cardiac structure, signalling, and inflammation.

Conclusions: PD-1 blockade induces cardiac dysfunction in mice with increased IL-17 signalling in the thymus. Pharmacological inhibition of IL-17A treatment prevents ICI-induced cardiac dysfunction.

KEYWORDS

cancer immunotherapy, cardio-oncology, cardiotoxicity, heart failure, nivolumab, pembrolizumab

1 | INTRODUCTION

Immune checkpoint inhibitors (ICI) have emerged as a novel form of cancer therapeutics in the past decade. ICIs have revolutionized the treatment of several malignancies, including metastatic melanoma, for which there has been limited therapeutic options beforehand (Gedye et al., 2015).

Malignant cells have multiple ways of evading the surveillance of the immune system, one of which is increasing the expression of immune checkpoints. Immune checkpoints, such as programmed cell death-1 (PD-1), programmed cell death-1 ligand (PD-L1), and cytotoxic T-cell antigen-4 (CTLA-4), are inhibitory molecules responsible for regulating T-cell activation and preventing autoimmunity in physiological conditions. ICIs enhance the cytotoxic effect of T-cells, leading to increased activation of the host immune system against cancer cells. However, enhanced T-cell activity may also cause immune-related adverse events (irAEs) in numerous organs, including the cardiovascular system (Postow et al., 2018).

ICI-associated cardiotoxicity includes myocarditis, which is a rare but often fatal adverse event, characterized by infiltration of CD4$^+$ and CD8$^+$ T-cells and CD68$^+$ macrophages (Johnson et al., 2016; Mahmood et al., 2018). ICI-induced myocarditis can present either with or without left ventricular dysfunction, and also may associate with arrhythmias (Hu et al., 2019). Other case reports have described non-inflammatory cardiac toxicities, such as a decline in cardiac function (Roth et al., 2016) and cardiomyopathy without concomitant myocarditis (Heinzerling et al., 2016), as well as Takotsubo-like syndrome, after treatment with

What is already known

- Immune checkpoint inhibitors may lead to immune related adverse events, including cardiovascular toxicities.

What does this study add

- Specific transcriptomic changes in the heart are associated with cardiotoxicity, due to PD-1 inhibition.
- PD-1 inhibition induces pro-inflammatory signalling in the thymus, while IL-17A inhibition prevents anti-PD-1-induced cardiac dysfunction.

What is the clinical significance

- Tumour-free patients receiving adjuvant ICI therapy may also be at risk of cardiotoxicity development.
- Repurposing IL-17 neutralizing antibodies could be a therapeutic option to prevent ICI-induced cardiotoxicity.

ICIs (Anderson & Brooks, 2016; Ederhy et al., 2018; Geisler et al., 2015). Importantly, late cardiac adverse events have been observed following ICI therapy, most commonly presenting as left ventricular systolic dysfunction and heart failure (Dolladille et al., 2020).

The clinical use of ICIs in cancer treatment is on the rise— between 2011 and 2018, the percentage of cancer patients eligible for ICI therapy increased from 1.54% to 46.6%, while there are hundreds of ongoing clinical trials investigating the use of ICIs in various cancer types (Zaha et al., 2020). Recently, a Danish nationwide study showed that cardiac adverse events in patients receiving ICI therapy are more frequent than previously thought, with a hazard ratio of up to 4.93 compared with non-ICI therapy (D'Souza et al., 2020). Therefore, identifying patients at risk, preventing and treating ICI-associated cardiovascular adverse events are key issues to address in the field of cardio-oncology. However, the molecular mechanisms of ICI-induced cardiotoxicity are not yet fully understood. In this study, we aimed to characterize ICI-induced cardiotoxicity in detail in preclinical models, to investigate the effect of ICI therapy on the cardiovascular system and its underlying mechanisms. Furthermore, we aimed to investigate pharmacological options to prevent the development of ICI-induced cardiac changes.

2 | METHODS

2.1 | Experimental animals and materials

Experimental procedures were carried out on male C57BL/6J mice and BALB/c (Oncological Research Center, Department of Experimental Pharmacology, Budapest, Hungary; and Janvier Labs, Le Genest-Saint-Isle, France), ranging from 8 to 10 weeks in age and weighing 20–28 g at the beginning of the study. These two mice strains exert a prototypical Th1- and Th2-type immune responses; accordingly, we carried out experiments on both strains. The animals had an acclimatization period of at least 1 week prior to experiments. Mice were maintained under a 12:12 h light–dark cycle, under controlled environmental conditions (20–24°C and 35–75% relative humidity) in individually ventilated cages (IVC) with shelters, holding two to three animals per cage. Standard rodent chow and tap water were provided ad libitum throughout the entire study. All procedures were approved by the National Scientific Ethical Committee on Animal Experimentation and the Semmelweis University's Institutional Animal Care and Use Committee (H-1089 Budapest, Hungary) in accordance with NIH guidelines (National Research Council [2011], Guide for the Care and Use of Laboratory Animals: Eighth Edition) and permitted by the government of Food Chain Safety and Animal Health Directorate of the Government Office for Pest County (project identification code: PE/EA/1912-7/2017; date of approval: November 2017). Animal studies are reported in compliance with the ARRIVE guidelines (Percie du Sert et al., 2020) and with the recommendations made by the *British Journal of Pharmacology* (Lilley et al., 2020). The following antibodies were used for in vivo treatment (all purchased from BioXCell, Lebanon, NH, USA): anti-PD-1 monoclonal antibody (clone RMP1-14, BP0146, RRID:AB_10949053), anti-CD4 (clone GK1.5, BP0003, RRID: AB_1107636), anti-IL17A (clone 17F3, BP0173, RRID: AB_10950102), and isotype control (rat IgG2a, clone 2A3, BP0089, RRID: AB_ 1107769).

2.2 | Experimental groups

C57BL/6J and BALB/c mice were randomly assigned to isotype control or anti-PD-1 treated groups, using a strategy to minimize initial weight difference between study groups. C57BL/6J mice were treated three times a week for either 2 or 4 weeks with a dose of 200 μg per mouse (n = 10 per group, Figure 1a), whereas BALB/c mice were treated for three times a week for 2 weeks with a dose of 200 μg per mouse (n = 10 per group, Figure 5a). Initial group size calculation was performed based on left ventricular ejection fraction (EF) as the primary endpoint. Assuming 65% as the control group's EF (based on previous measurements with typical standard deviation ±5), at least eight animals per group were needed to detect at least a 10% decrease with a power of 0.8 and alpha = 0.05. We selected 10 animals per group to account for unexpected mortality and technical issues. One mouse (C57BL/6J) was excluded from the study due to premature death, preventing the collection of echocardiographic and molecular/histological data, while another mouse (C57BL/6J) was excluded from conventional echocardiographic analysis due to technical issues. In separate experiments, C57BL6/J mice were randomly assigned to isotype control, anti-PD-1, anti-CD4, or anti-IL17A treated groups (200 μg per mouse, n = 10 per group, Figure 8a). One animal was excluded from the echocardiographic analysis due to technical issues. For all experiments, body weight was measured weekly. After the treatment period, cardiac function was evaluated by echocardiography. Following this, mice were killed under ketamine/xylazine anaesthesia (100/10 mg·kg⁻¹) with cervical dyslocation followed by whole-body perfusion with phosphate-buffered saline (PBS), after which organs were stored for histological and molecular analyses.

2.3 | Echocardiography

Mice were anaesthetised with isoflurane (5% for induction, 2% for maintenance) and placed on heating pads to maintain 37°C body temperature, with continuous monitoring of core temperature via a rectally placed probe. Echocardiographic analysis was done with the Vevo 3100 high-resolution in vivo imaging system (Fujifilm VisualSonics, Toronto, Canada) using an ultrahigh frequency MX400 transducer (30 MHz, 55 frames per second), by an operator blinded to the study groups. On two-dimensional recordings of the short-axis at the mid-papillary muscle level, measured parameters included left ventricular internal diameter in systole and diastole (LVIDs and LVIDd, respectively), LV anterior wall thickness and posterior wall thickness. End-diastolic and end-systolic LV areas were measured from short- and long-axis two-dimensional B-mode recordings. Diastolic parameters were measured in the apical four-chamber view. Pulse-wave Doppler and tissue Doppler were used to determine early mitral inflow velocity (E) and mitral annular early diastolic velocity (e′), respectively.

Fractional shortening was calculated as $[(LVIDd - LVIDs)/LVIDd] \times 100$. End-diastolic (LVEDV) and end-systolic (LVESV) LV
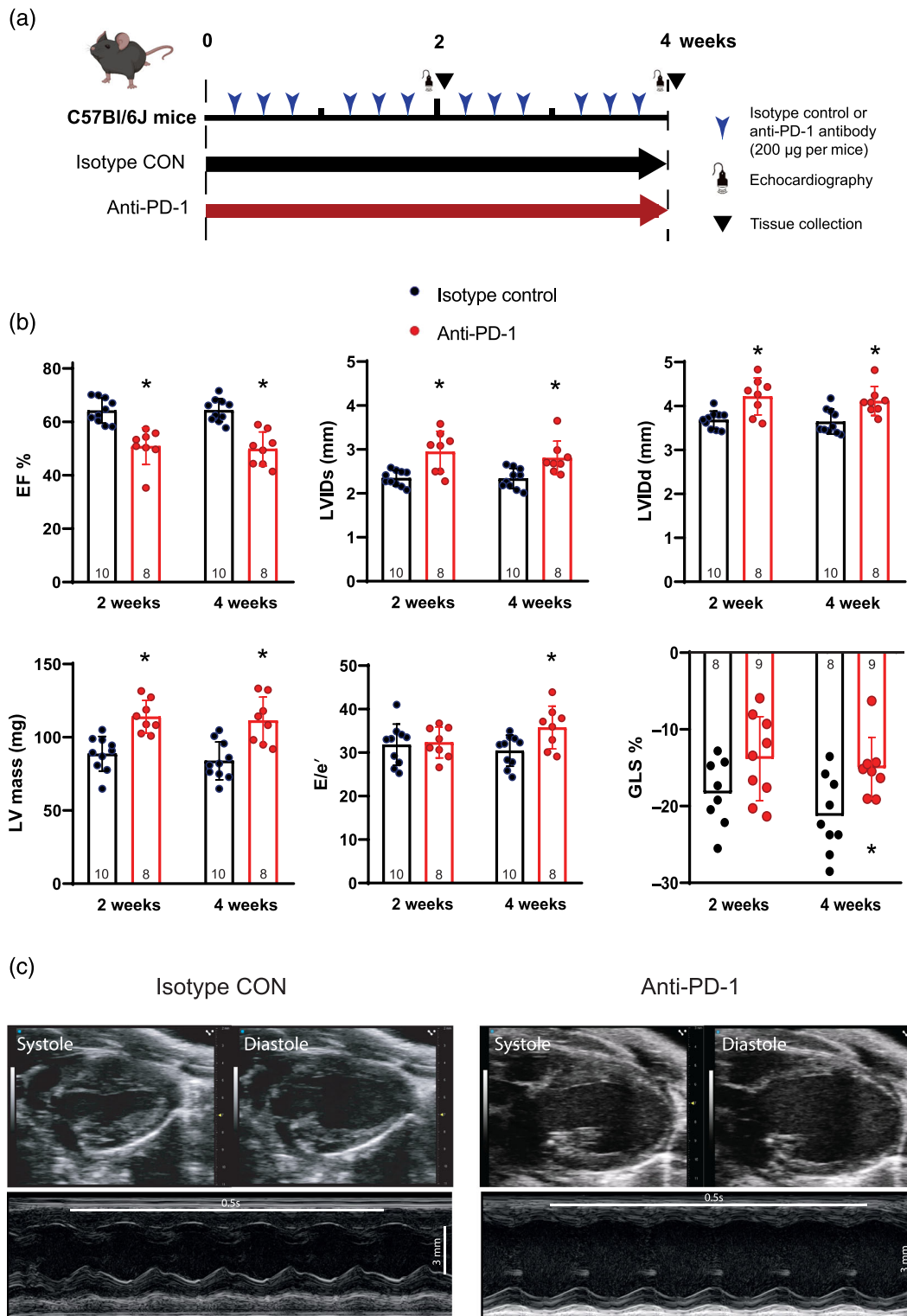
FIGURE 1 Cardiac function was impaired following anti-PD-1 treatment assessed by transthoracic echocardiography in C57BL/6J mice (black coat). (a) Study design for investigating the effects of anti-PD-1 treatment in C57BL/6J mice. Eight- to ten-week-old C57BL/6J mice were treated with isotype control or anti-PD-1 antibody for either 2 or 4 weeks, followed by echocardiography and tissue collection. (b) Selected parameters of systolic and diastolic function are shown. EF: ejection fraction; LV mass: left ventricular mass; LVIDs: left ventricular systolic internal diameter; LVIDd: left ventricular diastolic internal diameter, GLS: global longitudinal strain. *$P < 0.05$ versus time-matched isotype control, repeated measures ANOVA, followed by Bonferroni's post hoc test, n = 8–10 per group. (c) Representative echocardiographic B-mode and M-mode images of isotype control and anti-PD-1 treated animals. Scale bar: 3 mm. Time stamp: 0.5 s. Results are presented as mean ± standard deviation (SD). Exact group sizes are shown in each graph.

volumes were calculated from the rotational volumes of the left ventricular trace at the diastole and systole around the long axis line of the spline. Stroke volume (SV) was calculated as LVEDV − LVESV. Ejection fraction (EF) was determined as (SV/LVEDV) × 100. Cardiac output was calculated as (SV × HR/1000). LV mass was calculated according to a cubic formula, proposed first by Devereux et al. ([1986](#)) and modified for rodents (Zacchigna et al., [2021](#)) (LV mass = 1.04 [(LVIDd + LVAWd + LVPWd)^3 − LVIDd^3] × 0.8 + 0.6).

Echocardiographic recordings were evaluated via VevoLAB software (Fujifilm VisualSonics, Toronto, Canada) by an evaluator blinded to the study groups. Global longitudinal strain (GLS) was assessed by speckle-tracking. For this procedure, two to three consecutive cardiac cycles in B-Mode were selected. Using the Vevo Strain Software, semi-automated tracing of the endocardial and epicardial borders in the parasternal long-axis was performed to calculate GLS. Papillary muscles were excluded from GLS analysis. Mice with a high respiratory rate, which prevented tracing of consecutive cardiac cycles, were excluded from GLS analysis.

2.4 | Histologic analysis

Heart tissues were fixed in neutral buffered formalin for 24 h, then dehydrated in alcohols, and embedded in paraffin. Five-micrometre-thick sections were used for histological analyses and immunohistochemistry. All the stainings were visualized and images were captured with a Leica LMD6 microscope (Wetzlar, Germany).

2.4.1 | Haematoxylin and eosin staining

Paraffin-embedded heart sections were stained with haematoxylin and counterstained with eosin, after initial de-paraffinization and hydration for evaluation of morphologic and pathologic alterations.

2.4.2 | Sirius red staining

Heart sections after initial preparations (see above) were pre-treated with 0.2% aqueous phosphomolybdic acid, followed by staining with 0.0125% picrosirius red for 1 h, and then washed with 0.01 N HCl. The extent of cardiac fibrosis was analysed and quantified by ImageJ Software, using predefined threshold values, in a blinded manner.

2.4.3 | Immunohistochemistry

Prepared heart sections underwent antigen retrieval (Antigen Unmasking Solution, Citrate-based, pH = 6, Vector Laboratories, Newark, CA, USA, H-3300) for 30 min. Endogenous peroxidase activity was blocked by 3% H_2O_2 in PBS solution, and then the sections were blocked with 2.5% goat serum in PBS and 2.5% milk powder. Primary CD3ε antibodies (rabbit IgG, 85061, Cell Signaling

Technology, Leiden, The Netherlands, RRID:AB_2721019) and 3-nitrotyrosine (3-NT) antibodies (rabbit IgG, 06-284, EMD Millipore, Bedford, USA, RRID:AB_310089) were diluted (1:200) in goat serum (2.5%) and were incubated overnight at 4°C. After washing with gentle shaking three times with PBS, the sections were incubated with anti-rabbit IgG secondary antibodies (8114S, Cell Signaling Technology, Leiden, The Netherlands, RRID:AB_10544930) conjugated with horseradish peroxidase. Secondary antibodies were washed with gentle shaking three times with PBS and signals were developed with diaminobenzidine (SK-4103, ImmPACT DAB EqV Peroxidase [HRP] Substrate, Vector Laboratories, Burlingame, CA, USA, RRID:AB_2336521). CD3ε positive cells were counted manually by an evaluator blinded to study groups. 3-NT staining was analysed and quantified by ImageJ Software using predefined threshold values in a blinded manner. The immuno-related procedures used comply with the recommendations made by the British Journal of Pharmacology.

2.4.4 | Lectin histochemistry

Prepared heart sections underwent antigen retrieval (Antigen Unmasking Solution, Tris-based, pH = 9, Vector Laboratories, Newark, CA, USA, H-3301, RRID:AB_2336227) for 30 min. The sections were incubated with wheat germ agglutinin (WGA-FITC, 1:50, Sigma Aldrich, L4895) and isolectin B4 (ILB4-DyLight 594, 1:50, Invitrogen, L32473) overnight at 4°C. Cardiomyocyte cross sectional area was analysed by automatically delineating cross sections of cardiomyocytes with ImageJ Software, by an evaluator blinded to study groups. Cardiomyocytes were analysed on at least eight images per heart. Microvascular density was calculated as the ratio of microvascular count divided by the average cross-sectional area of the cardiomyocytes.

2.5 | RNA isolation and quantitative reverse transcription-polymerase chain reaction (qRT-PCR)

Total RNA was isolated from mouse heart, thymus, and spleen samples with a chloroform/isopropanol precipitation method. Briefly, Qiazol® (Qiagen, The Netherlands) was added to each sample and homogenized with TissueLyser (Qiagen, The Netherlands). Homogenates were centrifuged, and from the clean upper phase, DNA and protein were precipitated with chloroform. Total RNA was precipitated with isopropanol, and pellets were washed four times with 75% ethanol (vWR, PA, USA). Finally, total RNA was resuspended in nuclease-free water, and the RNA concentration was determined by spectrophotometry (Implen Nanophotometer® N60, München, Germany).

cDNA was synthesized from 1 μg total RNA by Sensifast cDNA synthesis kit (Bioline, UK) according to the manufacturer's protocol. cDNA was further diluted 20× with RNAse free water. qRT-PCR reactions were performed on a LightCycler® 480 II instrument (Roche, Germany) by using SensiFAST SYBR Green master mix (Bioline, UK).

Sequences of primers are shown in Table S1. **Peptidylprolyl isomerase A** (Ppia) and ribosomal protein L13a (Rpl13a) were used as housekeeping genes. Results were calculated with $2^{-\Delta\Delta Cp}$ evaluation method.

2.6 | RNA sequencing

The RNA Integrity Numbers and RNA concentration were determined by RNA ScreenTape system with 2200 Tapestation (Agilent Technologies, Santa Clara, CA, USA) and RNA HS Assay Kit with Qubit 3.0 Fluorometer (Thermo Fisher Scientific, Waltham, MA, USA), respectively.

For gene expression profiling (GEx) library construction, Quant-Seq 3' mRNA-Seq Library Prep Kit FWD for Illumina (Lexogen GmbH, Wien, Austria) was applied according to the manufacturer's protocol. The quality and quantity of the library was determined by using High Sensitivity DNA1000 ScreenTape system with the 2200 Tapestation (Agilent Technologies, Santa Clara, CA, USA) and dsDNA HS Assay Kit with the Qubit 3.0 Fluorometer (Thermo Fisher Scientific, Waltham, MA, USA), respectively. Pooled libraries were diluted to 2 pM for 1x86 bp single-end sequencing with 75-cycle High Output v2.5 Kit on the NextSeq 500 Sequencing System (Illumina, San Diego, CA, USA) according to the manufacturer's protocol. Datasets from the RNA sequencing experiments are publicly available at ArrayExpress (https://www.ebi.ac.uk/biostudies/arrayexpress) under the accession number E-MTAB-12388.

2.7 | Bioinformatics analysis of RNA sequencing data

To perform adapter and poly(A) tail trimming, quality- and length-filtering of raw RNA sequencing reads, we used Cutadapt software (version 2.10) (Martin, 2011). Reads with a Phred quality score below 30, or reads with a length of less than 19 nucleotides, were filtered out. For quality control analysis, we used FastQC (version 0.11.9) and MultiQC (version 1.10) (Ewels et al., 2016) tools. Adapter trimmed and filtered reads were aligned to the GRCm38 *Mus musculus* reference genome assembly (Ensemble release 81) (Yates et al., 2016) using HISAT2 software (version 2.2.1) (Kim et al., 2019). Annotation and read counting were performed by featureCounts (version 2.0.1) (Liao et al., 2014) using the corresponding reference annotation. Normalization, differential expression analysis of the annotated reads, and visualizations of the results by volcano plots were conducted with the use of the DESeq2 (version 1.10.1) (Love et al., 2014) Bioconductor package and custom scripts developed in the R programming language (version 3.2.3). To control false discovery rate due to multiple hypothesis testing, *P* values of pairwise comparisons were corrected by the Benjamini–Hochberg procedure yielding *q* values (Benjamini & Hochberg, 1995).

2.8 | Gene ontology enrichment analysis

We performed Gene Ontology (database version released on 9 October 2020) enrichment analysis against the *Mus musculus* reference gene list, using the online PANTHER Overrepresentation Test (geneontology.org, version released on 28 July 2020) (Mi et al., 2019) to evaluate enriched biological process terms among genes that were significantly differentially expressed based on non-corrected *P* values. Enrichment *P* values were assessed with Fisher's exact test, and results were corrected for multiple comparison by applying the false discovery rate method.

2.9 | Flow cytometry

Flow cytometry was performed to investigate the changes in lymphocyte populations following isotype control or anti-PD-1 treatment alone, or in combination with CD4 depletion or anti-IL17A. After 2 weeks of treatment in C57BL/6J mice, blood was drawn from the inferior vena cava in citrate-containing tubes, followed by collection of the thymus and spleen of animals. The thymus and spleen were manually dissected and homogenized through a 40-μm cell strainer (pluriStrainer 40 μm, Nylon-Mesh. 43-57040-51). The samples were centrifuged for 5 min at $400\times g$ and resuspended in 0.5- to 1-ml PBS. All samples were stained for 15 min with the following antibodies (all from Cell Signaling Technology, Leiden, The Netherlands, Mouse Activated T Cell Markers Flow Cytometry Panel, 62447): PE CD3 (28306), violetFluor 450TM CD4 (92599), PE-Cy7 CD8α (87922), FITC CD69 (39443), and PerCP-Cy5.5 CD25 (32325). The spleen and plasma samples were incubated with 1-ml red blood cell lysis buffer for 10 min (eBioscience™ 1X RBC Lysis Buffer, 00-4333-57). After washing steps, all samples were fixed in 2% PFA. A CytoFlex S flow cytometer (Beckman Coulter, Indianapolis, IN, USA) was used for data acquisition, and data were analysed using the CytExpert software (Beckman Coulter, Indianapolis, IN, USA) by an evaluator blinded to study groups.

2.10 | Statistical analysis

The data and statistical analysis comply with the recommendations of the *British Journal of Pharmacology* on experimental design and analysis in pharmacology (Curtis et al., 2018). All data were generated from at least five independent experiments. All values are presented as mean ± standard deviation (SD). The statistical analysis was performed using GraphPad Prism software (version 8.0.1). $P < 0.05$ was considered significant. Normal distribution of data was tested by the Shapiro–Wilk normality test. For comparisons between two groups, either parametric two-tailed Student's *t* test or nonparametric Mann–Whitney *U*-test was performed. Repeated measures ANOVA followed by Bonferroni's post hoc test was used for multiple comparisons between related groups. One-way ANOVA followed by

Tukey's post hoc test or Kruskal–Wallis test followed by Dunn's post hoc test was used to compare independent groups. The post hoc tests were conducted only if F in ANOVA or Kruskal–Wallis test achieved $P < 0.05$ and there was no significant variance inhomogeneity. For correlation analysis of two continuous variables, Spearman's rho (r_s) was computed, and 95% confidence intervals were obtained. ROUT analysis was performed to identify outliers, with Q value = 1%.

2.11 | Nomenclature of targets and ligands

Key protein targets and ligands in this article are hyperlinked to corresponding entries in http://www.guidetopharmacology.org and are permanently archived in the Concise Guide to PHARMACOLOGY 2021/22 (Alexander, Christopoulos, et al., 2021; Alexander, Cidlowski, et al., 2021; Alexander, Fabbro, Kelly, Mathie, Peters, Veale, Armstrong, Faccenda, Harding, Pawson, Southan, Davies, Annett, et al., 2021; Alexander, Fabbro, Kelly, Mathie, Peters, Veale, Armstrong, Faccenda, Harding, Pawson, Southan, Davies, Beuve, et al., 2021; Alexander, Kelly, Mathie, Peters, Veale, Armstrong, Faccenda, Harding, Pawson, Southan, Buneman, Cidlowski, Christopoulos, et al., 2021; Alexander, Kelly, Mathie, Peters, Veale, Armstrong, Faccenda, Harding, Pawson, Southan, Davies, Amarosi, Anderson, et al., 2021; Alexander, Mathie, et al., 2021).

3 | RESULTS

3.1 | Anti-PD-1 treatment leads to cardiac dysfunction and dilation of the left ventricle in C57BL/6J mice

Cardiac dysfunction has been associated with the use of immune checkpoint inhibitors, ranging from mild dysfunction to cardiogenic shock. Here, we investigated cardiac functional and morphological changes of C57BL/6J mice after 2 or 4 weeks of anti-PD-1 treatment using echocardiography (Figure 1).

Anti-PD-1 treatment has led to impaired systolic function in animals treated with PD-1 inhibitor, as shown by significantly decreased ejection fraction, while left ventricular mass was significantly increased compared with isotype control group (Figure 1b). On two-dimensional echocardiographic images of the anti-PD-1 treated animals, dilation of the left ventricle was seen compared with isotype controls (Figure 1c). This was quantitatively shown by increased left ventricular internal diameter at systole and diastole (LVIDs and LVIDd, respectively). Diastolic function was assessed by the ratio of early diastolic filling (E, measured via pulse-wave Doppler) and early diastolic mitral annular tissue velocity (e′, measured via tissue Doppler). E/e′ ratio correlates with the end-diastolic pressure of the left ventricle, which was significantly increased after 4 weeks of anti-PD-1 treatment. Global longitudinal strain (GLS) is a sensitive parameter showing early cardiac dysfunction. GLS was significantly

impaired due to anti-PD1 treatment after 4 weeks of treatment, while after 2 weeks, a tendency was seen ($P = 0.11$). Complete results of the echocardiographic measurements are shown in Table S2.

Altogether, immune checkpoint inhibition with a PD-1 inhibitor resulted in reduced cardiac systolic and diastolic function and led to left ventricular dilation.

3.2 | Anti-PD-1 treatment does not cause interstitial fibrosis or cardiomyocyte hypertrophy

Following the echocardiographic evaluation of cardiac function, the hearts were harvested for weight measurement, histological assessment, and molecular analysis. Similar to in vivo findings, representative histological sections of anti-PD-1 treated animals showed dilation of the ventricles (Figure 2a), while heart weight was significantly increased compared to isotype control groups (Figure 2b). Results of body and organ weight measurements are listed in Table S3. Cardiomyocyte cross-sectional area did not increase following anti-PD-1 treatment, and microvascular density also was unaffected (Figure 2c). In line with these findings, cardiac gene expression associated with hypertrophy did not reveal significant changes (Figure 2e). Anti-PD-1 treatment showed a mild tendency towards increased cardiac fibrosis, measured by either Sirius red staining (Figure 2d) or gene expression of fibrosis markers by qRT-PCR (Figure 2f).

Overall, it seems that cardiac hypertrophy and fibrosis did not increase significantly with anti-PD-1 treatment; thus, cardiac dysfunction and left ventricular dilation after anti-PD-1 treatment are likely the result of other mechanisms.

3.3 | Anti-PD-1 treatment leads to distinct transcriptomic profile of the heart

To investigate the underlying mechanisms of ICI-induced cardiac dysfunction, we aimed to characterize the transcriptomic changes occurring after anti-PD-1 treatment in the heart with bulk RNA sequencing. After 2 weeks of PD-1 inhibitor therapy, 538 genes were found to be differentially expressed after correcting for multiple comparisons, compared with isotype control treatment. Of these, 266 were up-regulated, and 272 were down-regulated. After 4 weeks of PD-1 inhibitor therapy, 55 genes were differentially expressed, with 17 being up-regulated and 38 down-regulated (Figure 3a). Figure 3b shows the 50 more significantly changed genes.

Furthermore, to analyse the functional changes after PD-1 inhibition, we performed Gene Ontology (GO) analysis. After 2 weeks of treatment, several GO terms related to cardiac contractile function were down-regulated, while GO terms indicating metabolic changes were found to be up-regulated. After 4 weeks, up-regulated genes with a high fold enrichment were related to antigen presentation via major histocompatibility complex (MHC) molecules (Figure 3c).
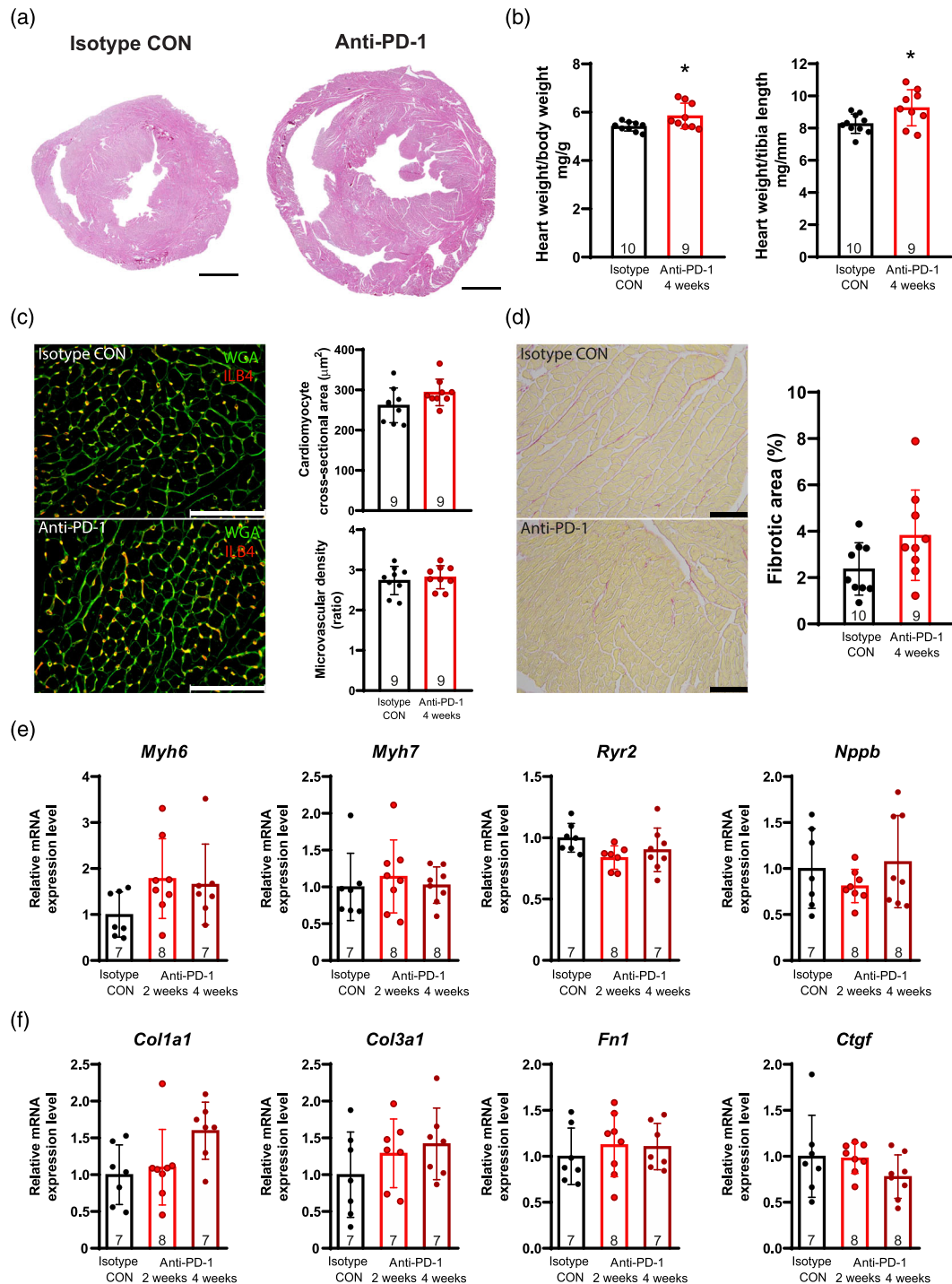
FIGURE 2 Concentric hypertrophy of the heart and cardiac fibrosis cannot explain the functional impairment and increase of heart weight following anti-PD-1 treatment. (a) Representative images of haematoxylin and eosin (H&E) stained hearts of isotype control and anti-PD-1 treated animals. Scale bar: 1 mm. (b) Comparison of heart weights relative to the body weight or tibia length of the animals. *$P < 0.05$ versus Isotype CON, Student's *t* test, n = 9–10 per group. (c) Cardiomyocyte cross-sectional area (CSA) was determined on WGA-stained sections (representative images are shown). Microvascular density was determined by the ratio of the microvascular number (stained with isolectin B4) and CSA. Scale bar: 100 μm. Student's *t* test: n.s., n = 9–10 per group. (d) Representative images are shown of hearts stained with Sirius red following anti-PD-1 treatment. Cardiac fibrosis is expressed as the ratio between the stained area and total area of the slice. Student's *t* test: n.s., n = 9–10 per group. Scale bar: 100 μm. (e, f) qRT-PCR was performed to assess relative expression of hypertrophy- (e) and fibrosis-related (f) genes. One-way ANOVA or Kruskal–Wallis test was performed, followed by Tukey's or Dunn's post hoc test if the test's *P* value was significant, n = 7–8 per group. Results are presented as mean ± standard deviation (SD). Exact group sizes are shown in each graph.

FIGURE 3 RNA sequencing shows distinct myocardial transcriptomic profile after anti-PD-1 treatment in C57BL/6J mice. (a) Volc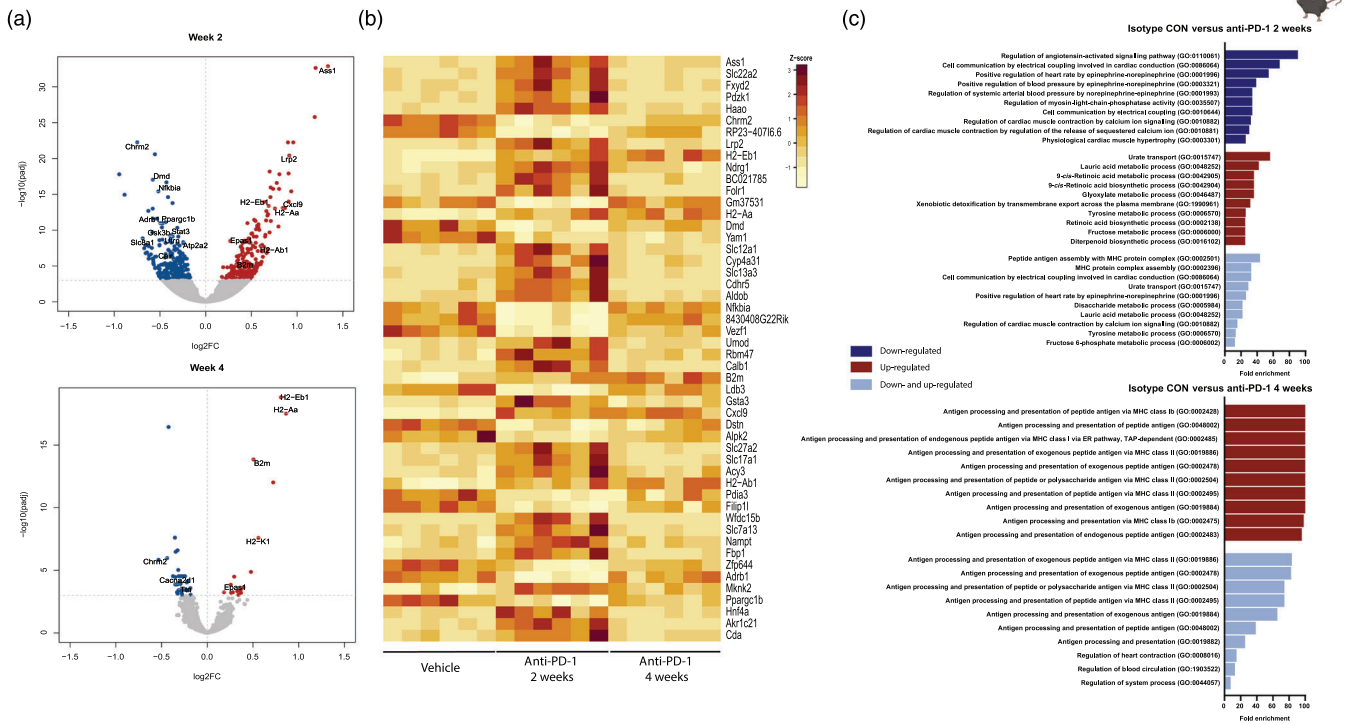ano plots showing down- and up-regulated genes after 2 and 4 weeks of anti-PD-1 treatment. (b) Heat map showing gene-wise Z-scores of the normalized read counts of the 50 most significant differentially expressed genes after 2 and 4 weeks of anti-PD-1 treatment. (c) Gene ontology (GO) biological process enrichment analysis of the differentially expressed transcripts following 2 and 4 weeks of anti-PD-1 treatment (a and b, respectively), compared with isotype control. GO terms were categorized based on their expression pattern (down-regulated, up-regulated, and down- and up-regulated). The top 10 GO terms with the highest fold enrichment values are shown in each category. All of the shown GO terms had adjusted P values < 0.05 and were considered significant. n = 6 animals per group.

Altogether these findings indicate that immune checkpoint inhibition with anti-PD-1 treatment leads to a distinct transcriptomic profile, characterized by reduced cardiac contractility, metabolic changes, and increased antigen presentation.

3.4 | Anti-PD-1 treatment increases myocardial nitrosative stress via increased Nox2 expression

Increased nitrosative stress by peroxynitrite formation has been shown to induce cardiac dysfunction (Pacher et al., 2005). Thus, we aimed to investigate the role of nitrosative stress in ICI-induced cardiotoxicity. We measured the level of 3-nitrotyrosine (3-NT immunohistochemistry), an in vivo marker of oxidative damage mediated by peroxynitrite. 3-NT formation was increased transiently after 2 weeks of anti-PD-1 treatment, compared with isotype control and with 4 weeks of anti-PD-1 treated groups (Figure S1A,B). **NADPH-oxidases** and **nitrogen monoxide synthases** (NOS) are responsible for increased superoxide and/or nitric oxide production, leading to peroxynitrite generation. Expression of *Nox2* was found to be increased after 2 and 4 weeks of anti-PD-1 treatment, while other oxidase subunits (*p22phox* and *Nox4*) and NO-synthases (*Nos1*, *Nos2*, and *Nos3*) were not altered by the treatment (Figure S1C).

3.5 | Anti-PD-1 treatment leads to systemic inflammatory activation without local T-cell infiltration in the heart

Next, we studied the inflammatory changes following anti-PD-1 treatment. In clinical cases, ICI therapy has been associated with T-cell and macrophage infiltration of the myocardium, resulting in autoimmune myocarditis (Johnson et al., 2016). To investigate the potential pro-inflammatory effects of anti-PD-1 treatment in the development of cardiac dysfunction, we measured the changes of inflammatory gene expression locally (in the heart) and remotely (in the thymus and spleen) via qRT-PCR (Figure 4). Anti-PD-1 treatment significantly increased the expression of *Il1b* in the heart after 2 weeks, whereas *Aif1* and *Cd163*—markers of different macrophage populations—were increased after 4 weeks of PD-1 inhibitor treatment. However, other cytokines, or cell-type specific markers of inflammation, were not affected significantly, including *Cd3e* expression (Figure 4a). Furthermore, CD3ε immunohistochemistry did not show an increase in the numbers of CD3^{+} T-cells in the myocardium (Figure 4b).

Immune checkpoint inhibition has also been reported to cause various systemic immune-related adverse effects. The thymus plays a vital role in the development of T-cells; thus, we investigated the effect of anti-PD-1 treatment on thymic inflammatory gene

expression. Accordingly, we found increased levels of pro-inflammatory cytokines (*Il3*, *Il6*, *Il17A*, *Il17F*, and *Il23*) (Figure 4c). Of these, *Il17a* showed the highest increase compared with the isotype control-treated group. Importantly, gene expression of anti-inflammatory cytokine *Il10* did not change significantly, leading to increased *Il17a/Il10* ratio after anti-PD-1 treatment. Furthermore, we also assessed inflammatory changes in the spleen, where only *IFNG* showed increased expression after 2 weeks of anti-PD-1 treatment (Figure 4d).

Altogether, these findings indicate that cardiac dysfunction after anti-PD-1 treatment in healthy C57BL/6J mice can develop independently of T-cell infiltration into the myocardium. However, gene expression of pro-inflammatory cytokines is markedly increased in the thymus, and to a lesser extent in the spleen, suggesting remote cytokine production as a potential mediator of ICI-induced cardiac dysfunction.

3.6 | Anti-PD-1 treatment does not cause cardiac dysfunction in BALB/c mice

Following the findings that anti-PD-1 treatment induced pro-inflammatory gene expression in the thymus, we investigated the effect of PD-1 inhibition in BALB/c mice, which are known to differ in systemic T-cell mediated immune response (Watanabe et al., 2004). Because we saw the most prominent changes in cardiac gene expression after 2 weeks of treatment in C57BL/6J mice, we treated BALB/c mice for 2 weeks with isotype control or with anti-PD-1 (Figure 5a). In contrast to C57BL/6J mice, BALB/c mice did not show increased heart weight, nor left ventricular dilation, nor cardiac dysfunction following PD-1 inhibition (Figure 5b–e), suggesting that this strain of mice is resistant to anti-PD-1 inhibition induced cardiac dysfunction in this experimental setting.

3.7 | Comparison of inflammatory and molecular changes induced by PD-1 inhibition in the hearts of C57BL/6J and BALB/c mice

We hypothesized that by investigating molecular changes due to anti-PD-1 treatment in BALB/c mice, we could identify discrepancies compared with the response seen in C57BL/6J mice, which then could provide insights into the molecular events of ICI-induced cardiac dysfunction development.

First, we investigated inflammatory changes in BALB/c mice. In the heart, the expression of *Il4* and *Cd163* increased significantly, while in contrast to C57BL/6J mice, *Il1b* expression was not altered (Figure 6a). In the thymus, we have seen a prominent response to anti-PD-1 treatment, with the increase of *Il3*, *Il6*, *Il10*, *Il17a*, *Il17f*, *Il23*, *Rora*, and decrease of *Il4* and *Gata3*. Interestingly, opposed to C57BL/6J mice, expression of anti-inflammatory cytokine *Il10* was significantly increased, leading to a lower ratio of *Il17a/Il10* (Figure 6b).

Next, we analysed nitrosative stress in the heart of BALB/c mice, in which nitrosative stress was increased significantly in C57BL/6J mice after 2 weeks of anti-PD-1 treatment. Here, we did not find any alteration of 3-NT immunohistochemistry staining (Figure S2A,B). *Nox2* was significantly up-regulated (Figure S2C), albeit the magnitude of increase was lower compared with C57BL/6J mice.

Lastly, we aimed to validate the gene expression changes in the heart identified by bulk RNA sequencing in C57BL/6J mice via qRT-PCR, and compare them with changes in the hearts of BALB/c mice. Of the most significantly altered genes in the hearts of C57BL6/J, we selected 15 genes through literature search that have been shown previously to play potential roles in cardiac inflammation and/or dysfunction. We identified nine genes that were significantly up- or down-regulated compared with isotype control in C57BL/6J mice measured via qRT-PCR, in accordance with the RNAseq results (Figure 7a). Of these genes, *Dmd*, *Chrm2*, *Nfkbia*, *Stat3*, *Gsk3b*, and *Ldb3* were significantly down-regulated, while in BALB/c mice, these genes were significantly up-regulated. *Fxyd2* and *Cxcl9* were up-regulated in C57BL/6J mice, although they did not change significantly in BALB/c mice. Correlation analysis showed significant positive correlation between gene expression and left ventricular ejection fraction in the case of *Dmd*, *Ldb3*, *Chrm2*, *Nfkbia*, *Stat3*, and *Gsk3b*, while negative correlation was found in the case of *Fxyd2* and *Ass1* (Figure 7b).

3.8 | Anti-IL17A treatment or CD4 T-cell depletion prevents the development of anti-PD-1 induced cardiac dysfunction

After the molecular characterization of ICI-induced cardiac dysfunction, we further investigated mechanisms that could be targeted pharmacologically to alleviate anti-PD-1-induced cardiotoxicity. Our previous results showed that expression of several pro-inflammatory cytokines increased after anti-PD-1 treatment. Thus, first we depleted CD4+ T-cells, which are major contributors to cytokine production. Since the expression of *Il17a* was most prominently induced by PD-1 inhibition, we also targeted IL-17A with a monoclonal antibody as a clinically relevant intervention. We found that the depletion of CD4+ T-cells, and selective blockade of IL-17A, prevented the development of ICI-induced cardiac dysfunction, as shown by maintained ejection fraction in the respective groups, whereas the ejection fraction was decreased with anti-PD-1 treatment alone (Figure 8b). The efficacy of CD4+ T-cell depletion was confirmed by flow cytometry of T-cells harvested from the spleen and thymus (Figure 8d), as well as from venous blood (Figure S3B). Interestingly, treatment with anti-PD-1 antibody alone, or in combination with anti-IL17A, modestly decreased the CD4+ T-cell population in the spleen (Figure 8d). T-cell activation marker CD69 was decreased in the thymus of the CD4+ T-cell depleted animals, compared with the isotype control treated group, but were not altered with anti-PD-1 or anti-IL17A treatments, while **CD25** was not affected by either treatment (Figure S3C).
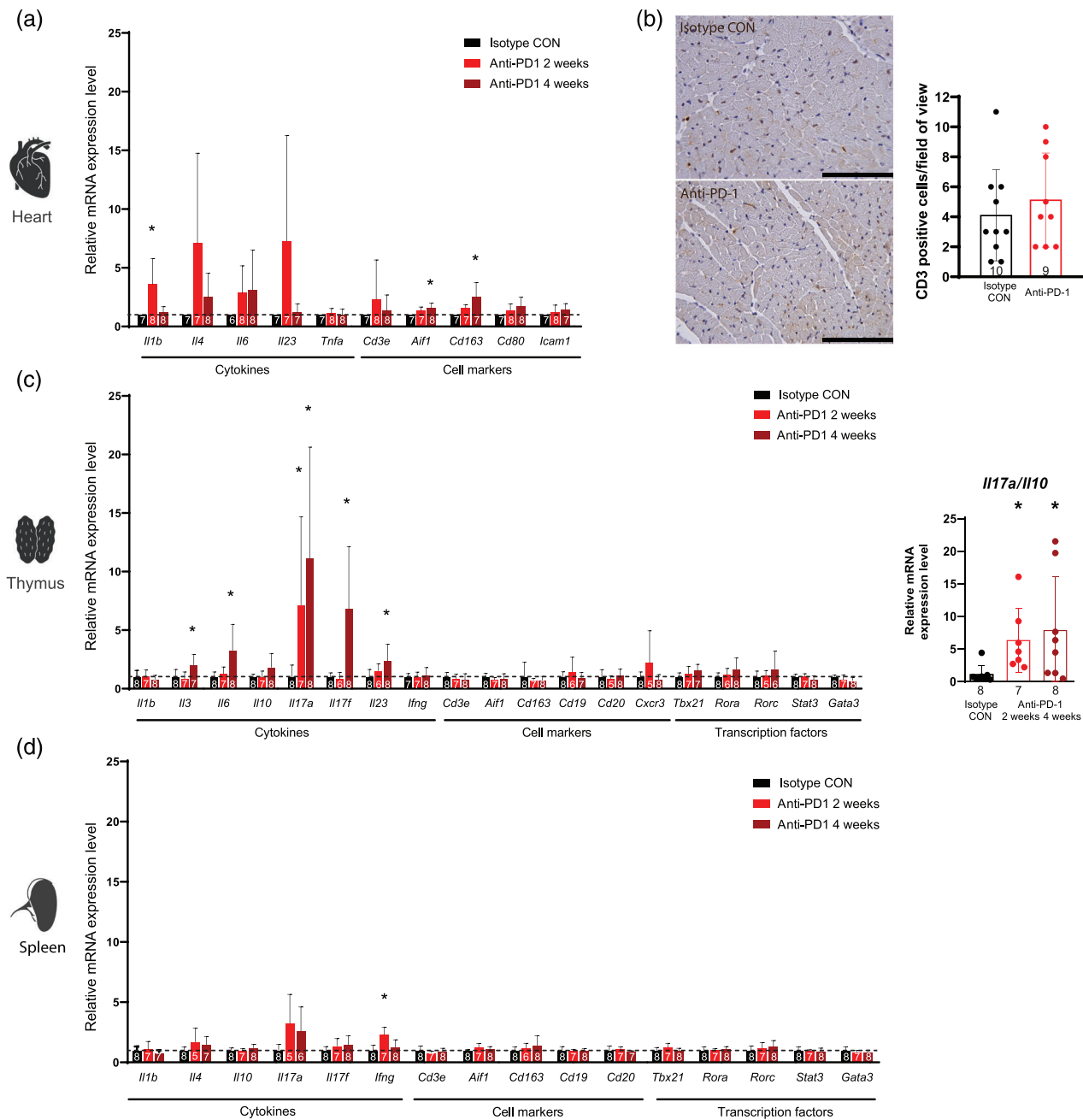
FIGURE 4 Anti-PD-1 treatment causes mild inflammation in the heart and prominent inflammatory gene expression in the thymus of C57BL/6J mice. (a) Analysis of mRNA expression of cytokines (*Il1b*, *Il4*, *Il6*, *Il23*, and *Tnfa*) and cell markers (*Cd3e*, *Aif1*, *Cd163*, *Cd80*, and *Icam1*) in the heart by qRT-PCR. *$P < 0.05$ versus Isotype CON, one-way ANOVA or Kruskal-Wallis test followed by Tukey's or Dunn's post hoc test, n = 6–8 per group. (b) Representative images and quantification of CD3ε immunohistochemistry after anti-PD-1 treatment. Scale bar: 100 μm. Student's *t* test: n.s., n = 9–10 per group. (c) Analysis of mRNA expression of cytokines (*Il1b*, *Il3*, *Il6*, *Il10*, *Il17a*, *Il17f*, *Il23*, and *Ifng*), cell markers (*Cd3e*, *Aif1*, *Cd163*, *Cd19*, *Cd20*, and *Cxcr3*), and transcription factors (*Tbx21*, *Rora*, *Rorc*, *Stat3*, and *Gata3*) in the thymus by qRT-PCR. *$P < 0.05$ versus Isotype CON, one-way ANOVA or Kruskal-Wallis followed by Tukey's or Dunn's post hoc test, n = 6–8 per group. (d) Analysis of mRNA expression of cytokines (*Il1b*, *Il4*, *Il6*, *Il10*, *Il17a*, *Il17f*, and *Ifng*), cell markers (*Cd3e*, *Aif1*, *Cd163*, *Cd19*, and *Cd20*), and transcription factors (*Tbx21*, *Rora*, *Rorc*, *Stat3*, and *Gata3*) in the spleen by qRT-PCR. *$P < 0.05$ versus Isotype CON, one-way ANOVA or Kruskal-Wallis test followed by Tukey's or Dunn's post hoc test, n = 6–8 per group. Results are presented as mean ± standard deviation (SD). Exact group sizes are shown in each graph.
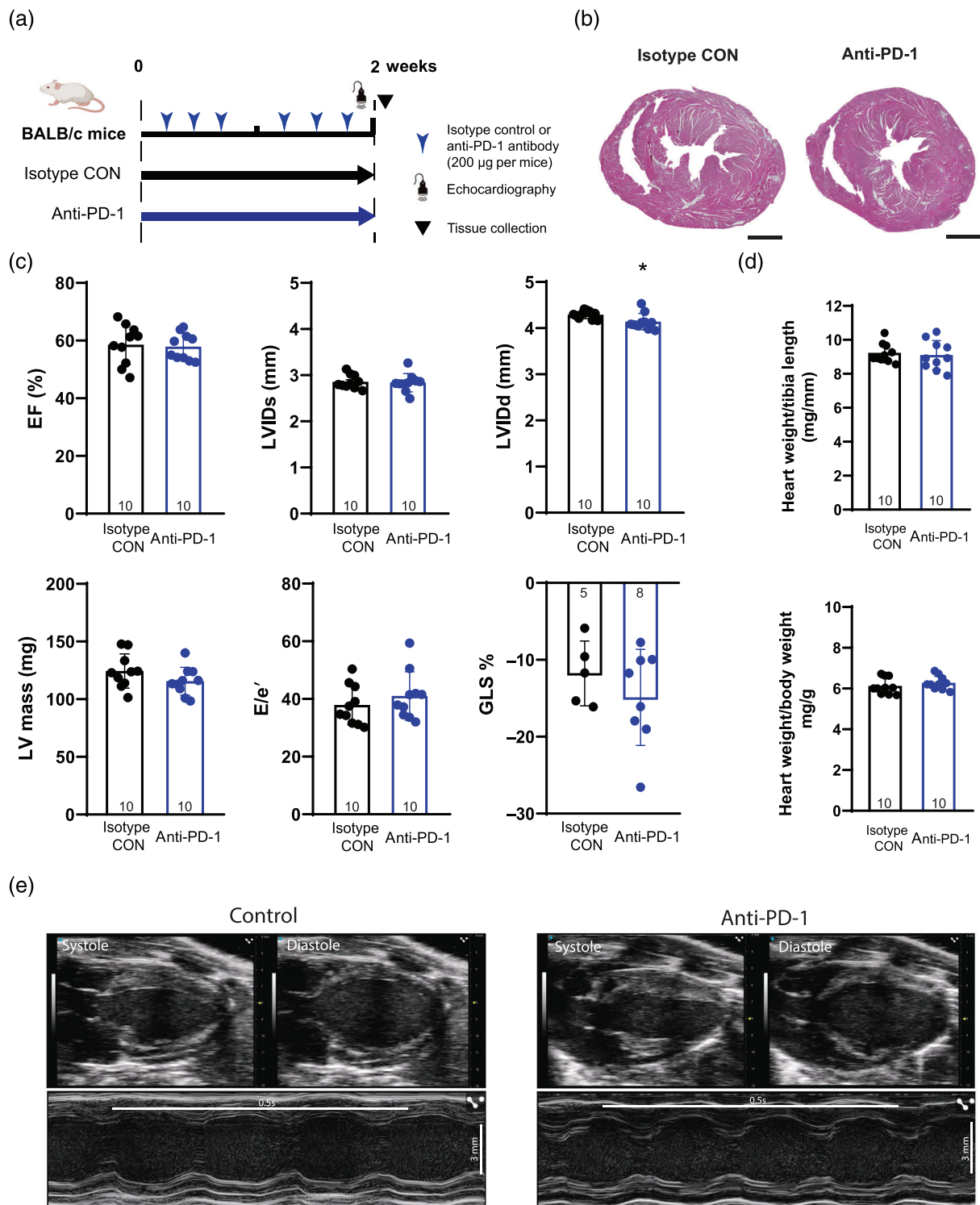
FIGURE 5 Anti-PD-1 treatment does not cause cardiac dysfunction or left ventricular dilation in BALB/c mice (albino, white coat). (a) Study design for investigating the effects of anti-PD-1 treatment in BALB/c mice. Eight- to ten-week-old BALB/c mice were treated with isotype control or anti-PD-1 antibody for 2 weeks, followed by echocardiography and tissue collection. (b) Representative images of hematoxylin and eosin (H&E) stained hearts of isotype control and anti-PD-1 treated animals. Scale bar: 1 mm. (c) Selected parameters of systolic and diastolic function are shown. EF: ejection fraction; LV mass: left ventricular mass; LVIDs: left ventricular systolic internal diameter; LVIDd: left ventricular diastolic internal diameter; GLS: global longitudinal strain. *$P < 0.05$ versus isotype control, Student's two-tailed t test, n = 10 per group for quantification of EF, LVIDs, LVIDd, LV mass, E/e′, n = 5–8 per group for quantification of GLS. (d) Comparison of heart weights relative to the body weight or tibia length of the animals. *$P < 0.05$ versus Isotype CON, Student's t test, n = 10 per group. (e) Representative echocardiographic B-mode and M-mode images of isotype control and anti-PD-1 treated animals. Scale bar: 3 mm. Time stamp: 0.5 s. Results are presented as mean ± standard deviation (SD). Exact group sizes are shown in each graph.
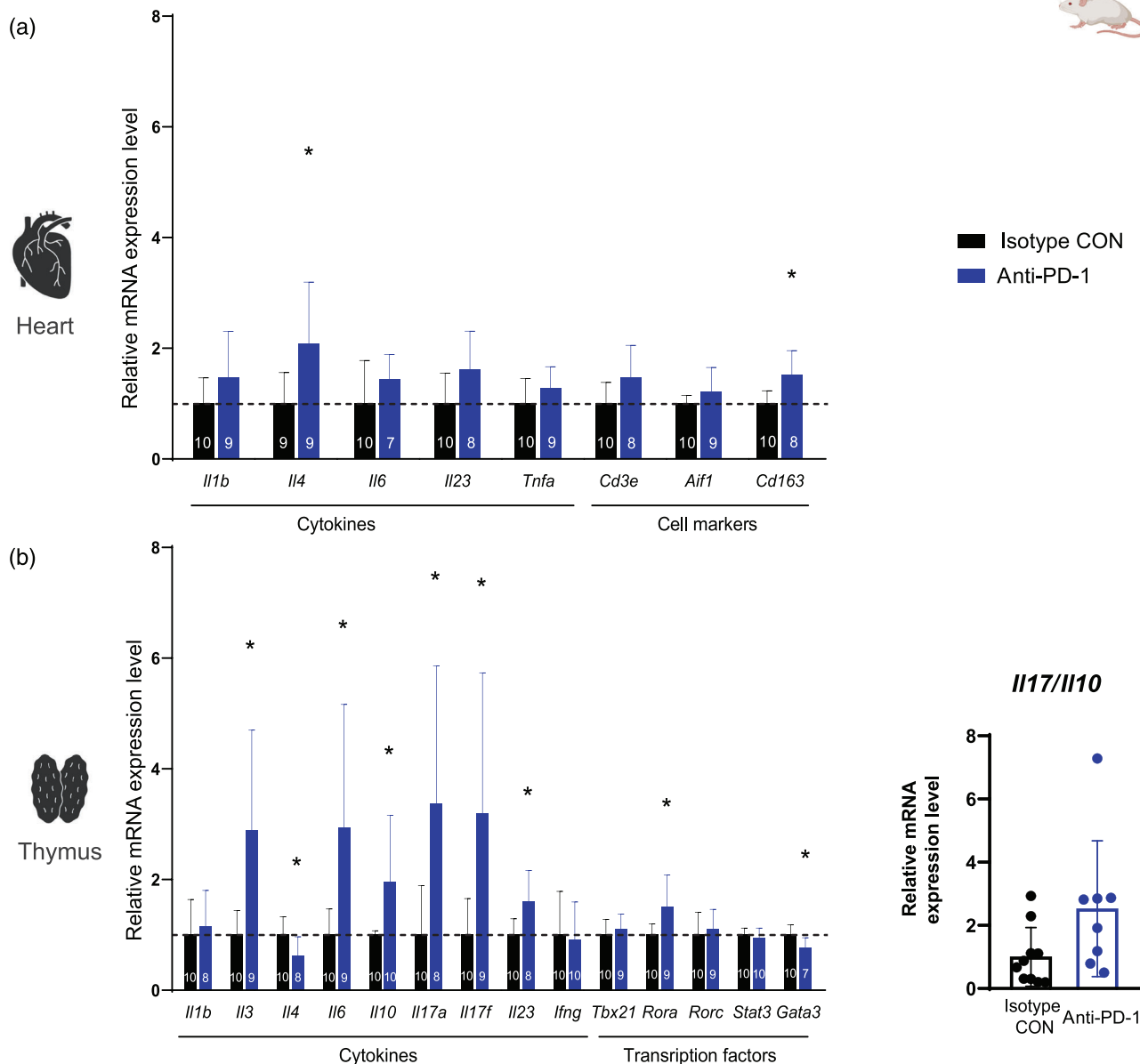
FIGURE 6 Investigation of anti-PD-1 induced inflammatory changes in BALB/c mice. (a) Analysis of mRNA expression of cytokines (*Il1b*, *Il4*, *Il6*, *Il23*, and *Tnfa*) and cell markers (*Cd3e*, *Aif1*, *Cd163*, *Cd80*, and *Icam1*) in the heart by qRT-PCR. *$P < 0.05$ versus Isotype CON, Student's *t* test or Mann-Whitney *U*-test, n = 7–10 per group. (b) Analysis of mRNA expression of cytokines (*Il1b*, *Il3*, *Il6*, *Il10*, *Il17a*, *Il17f*, *Il23*, and *Ifng*), cell markers (*Cd3e*, *Aif1*, *Cd163*, *Cd19*, *Cd20*, and *Cxcr3*) and transcription factors (*Tbx21*, *Rora*, *Rorc*, *Stat3*, and *Gata3*) in the thymus by qRT-PCR. *$P < 0.05$ versus Isotype CON, Student's *t* test or Mann-Whitney *U*-test, n = 7–10 per group. Results are presented as mean ± standard deviation (SD). Exact group sizes are shown in each graph.

4 | DISCUSSION

In this study, we demonstrate that anti-PD-1 treatment leads to cardiac contractile dysfunction in C57BL/6J mice, characterized by left ventricular dilation with systolic and diastolic dysfunction. In contrast, BALB/c mice did not develop cardiac dysfunction nor dilation of the left ventricle. In both strains, anti-PD-1 treatment was associated with only smouldering inflammatory changes in the heart; however, there was prominent activation of thymic cytokine expression. Of note, C57BL/6J

mice presented with an increased *Il17a/Il10* ratio, whereas increased *Il10* production was seen in BALB/c mice, indicating a more balanced thymic activation. Depletion of CD4$^+$ T-cells or inhibition of IL-17A prevented the development of anti-PD-1-induced cardiac dysfunction in C57BL/6J mice. Investigating the cardiac gene expression changes in both strains revealed differentially regulated genes, providing mechanistic insights into the development of ICI-induced cardiac dysfunction.

Several forms of cardiotoxicity have been described previously as a result of ICI therapy. Of these, myocarditis, a rare but often fatal

(a)
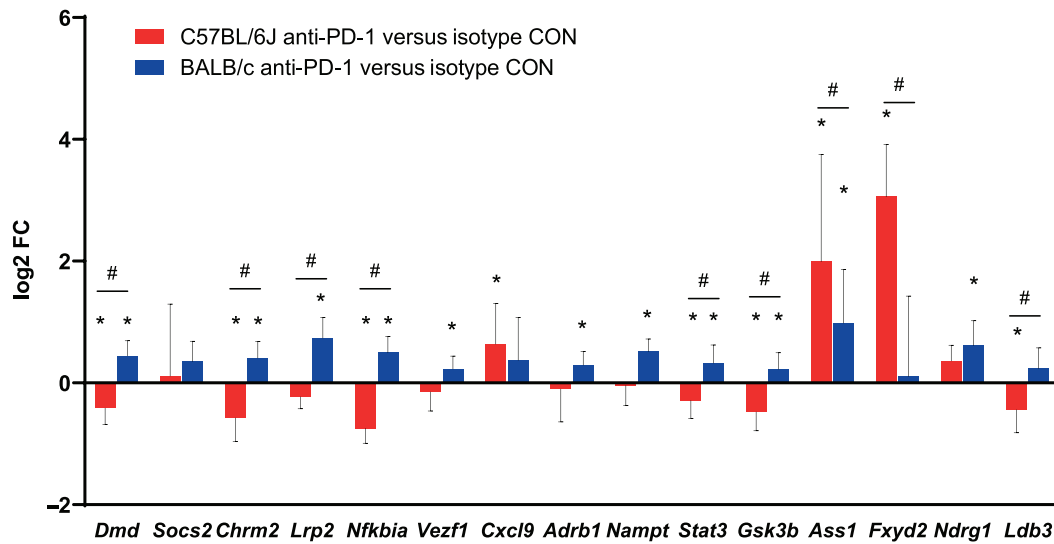
(b)
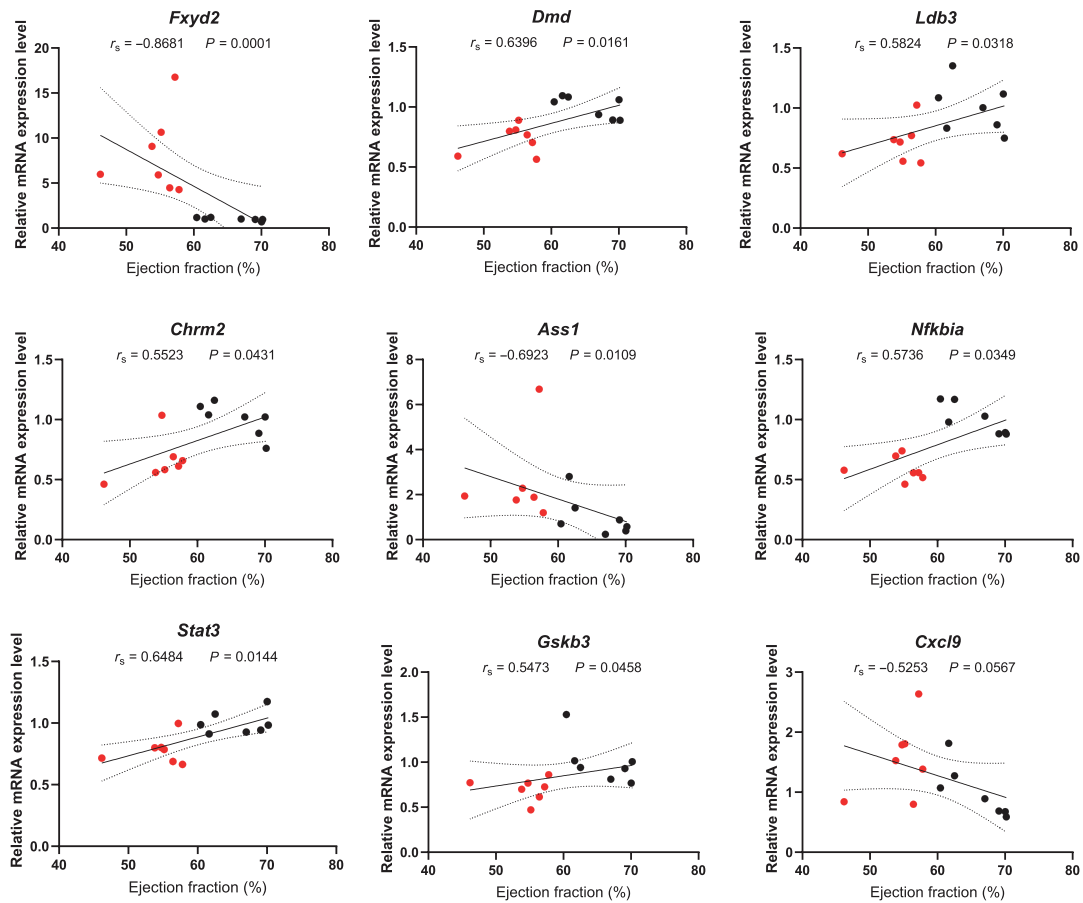
FIGURE 7 Comparison of molecular changes in the hearts of C57BL/6J and BALB/c mice following 2 weeks of anti-PD-1 treatment. (A) Analysis of cardiac gene expression by qRT-PCR. *P < 0.05 versus corresponding isotype CON, Student's *t* test or Mann-Whitney *U*-test, n = 6–10 per group. #P < 0.05 between C56BL/6J and BALB/c groups, Student's *t* test, n = 6–10 per group. (B) Correlation analysis between expression level of cardiac genes and left ventricular ejection fraction in C57BL/6J mice, Spearman's correlation test. Red dots indicate animals treated with anti-PD-1, while black dots show isotype control treated mice. Results are presented as mean ± standard deviation (SD).
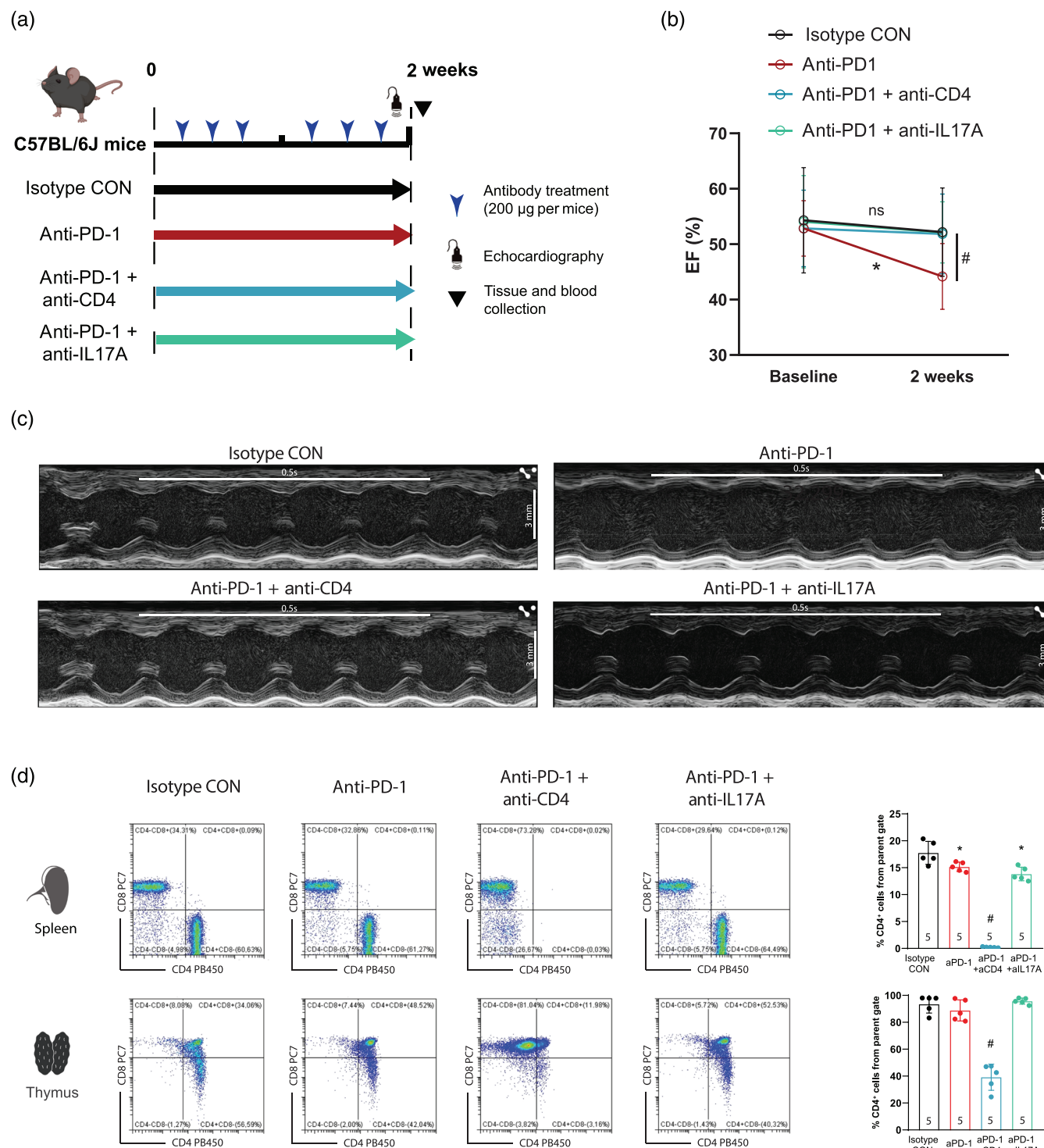
FIGURE 8 Anti-PD-1-induced cardiac dysfunction is prevented by co-treatment with anti-CD4 or anti-IL17A antibody. (a) Study design for investigating the effects of anti-CD4 and anti-IL17A co-treatment with anti-PD-1 in C57BL/6J mice. (b) Treatment with anti-CD4 or anti-IL17A prevented the decline in ejection fraction seen with anti-PD-1 treatment alone. *$P < 0.05$ versus corresponding baseline, repeated measures ANOVA, followed by Bonferroni's post hoc test. #$P < 0.05$ versus anti-PD-1 at 2 weeks, repeated measures ANOVA, followed by Dunnett's post hoc test, n = 9 for isotype CON group, n = 10 for anti-PD-1, anti-PD-1 + anti-CD4, and anti-PD-1 + anti-IL17A groups. Results are presented as mean ± standard deviation (SD). (c) Representative echocardiographic M-mode images of isotype control, anti-PD-1, anti-PD-1 + anti-CD4, and anti-PD-1 + anti-IL17A treated animals. Scale bar: 3 mm. Time stamp: 0.5 s. (d) Representative flow cytometry images and quantification of CD4^{+} cells in the spleen and thymus of isotype control, anti-PD-1, anti-PD-1 + anti-CD4, and anti-PD-1 + anti-IL17A treated animals. Gating strategy for flow cytometry analysis is shown in Figure S3. *$P < 0.05$ versus isotype CON, one-way ANOVA, followed by Tukey's post hoc test. #$P < 0.05$ versus isotype CON, anti-PD-1, and anti-PD-1 + anti-IL17A groups, one-way ANOVA, followed by Tukey's post hoc test, n = 5 per group. Results are presented as mean ± standard deviation (SD).

adverse event, has been the most extensively investigated in clinical studies and preclinical models. However, accumulating evidence suggests, that besides myocarditis, ICI therapy leads to increased occurrence of other cardiovascular diseases, such as accelerated atherosclerosis (Drobni et al., 2020) and heart failure (Dolladille et al., 2020). In retrospective investigations, left ventricular systolic dysfunction has been associated with prior ICI treatment (Escudier et al., 2017) (Michel et al., 2022). Based on these findings, subclinical cardiac dysfunction may be a common manifestation of ICI-induced cardiotoxicity, and it may affect a significant proportion of patients treated with ICIs, highlighting the need to investigate the effect of immune checkpoint inhibitors on cardiac function and its underlying mechanisms.

The interaction between cancer and the immune system also may play an important role in triggering ICI-related adverse events. In preclinical reports, anti-PD-1 treatment of B16-F10 melanoma-bearing BALB/c mice resulted in decreased cardiac function and inflammation in the heart, whereas there were no differences found in the non-tumour bearing groups (Tay et al., 2020), in agreement with our findings, where non-tumour bearing BALB/c mice were resistant to PD-1 induced cardiotoxicity. However, in an early study by Nishimura et al. (2001), PD-1 deletion in BALB/c mice resulted in severe dilated cardiomyopathy, suggesting that PD-1 plays a role in maintaining cardiac homeostasis, and that genetic interference with PD-1 signalling may cause cardiac disturbances even without tumour presence. Michel et al. (2022) have found that only tumour-bearing C57BL/6 mice developed cardiac dysfunction after 13 days of anti-PD-1 administration; however, this is in contrast to our findings, where non-tumour bearing C57BL/6J mice developed dysfunction even after 2 weeks of treatment. An interesting difference in the study by Michel et al. (2002) is that female mice were treated, as opposed to male mice in our experiments, which could suggest sex-mediated differences in the response to anti-PD-1 treatment. Our findings that PD-1 inhibition without tumour presence causes significant cardiac dysfunction highlights the fundamental role of the PD-1–PD-L1 immune checkpoint system in maintaining cardiac physiology. Therefore, tumour-free patients treated with adjuvant ICI therapy to prevent recurrence (Weber et al., 2017) may still be at risk for ICI-induced cardiotoxicity.

Interestingly, despite evident changes in cardiac function, only mild inflammation was found in the heart in our present study. Thus, it is highly likely that the decrease in cardiac function after anti-PD-1 treatment could not be fully explained by myocardial T-cell infiltration and local cytokine production. However, ICIs are known to cause systemic immune stimulation and adverse events. Thus, we hypothesized that T-cell activation in remote immune-related organs and subsequent remote cytokine production may mediate the observed cardiac dysfunction. Enhanced thymic activity following immune checkpoint inhibition has been shown previously in a case report, where thymic hyperplasia has been observed in patients (Mencel et al., 2019). Furthermore, ICI treatment of patients with thymoma has been associated with the development of myocarditis (Konstantina et al., 2019). Increased cytokine production by T-cells activated in the thymus may lead to cardiac dysfunction even without massive inflammatory cell infiltration into the myocardium, for example, by cytokine-induced peroxynitrite formation (Ferdinandy et al., 2000), which corresponds with our present findings of increased nitrosative stress in the myocardium.

Of note, in our study, *Il17a* showed the highest increase in the thymus of C57BL/6J mice. IL-17 is a pro-inflammatory cytokine produced primarily by Th17 cells. In clinical studies, the level of circulating IL-17 was found to correlate with ICI-induced colitis (Tarhini et al., 2015). In accordance with this finding, in human peripheral blood cells, anti-PD-1 treatment increased IL-17 production in vitro (Dulos et al., 2012), while increased Th17 subpopulations were associated with inflammatory and autoimmune toxicities following immune checkpoint inhibition (von Euw et al., 2009). In a mouse model of experimental autoimmune myocarditis (EAM), IL-17A was associated with ventricular dilation and dysfunction after myocarditis, but not with myocarditis development per se (Baldeviano et al., 2010), corresponding with our findings that cardiac dysfunction occurred without significant local inflammation in the heart, with increased systemic IL-17A expression. Further strengthening the link between heart failure development and IL-17, Myers et al. (2016) found that myocarditis/DCM patients with subsequent heart failure (NYHA III-IV) had significantly higher serum IL-17 levels compared with NYHA I-II patients. Similarly, increased IL-17 serum concentration was found in patients with heart failure, as well as in a mouse model of pressure-overload induced heart failure, where IL-17 knock-out improved cardiac function (Xue et al., 2021). Based on the finding that systemic inflammatory gene expression was altered by anti-PD-1 treatment, primarily in the thymus, we speculated that PD-1 inhibition would have different effects in mice with different systemic immune response. BALB/c mice exert a Th2-dominant immune response, as opposed to C57BL/6J mice. In accordance with our hypothesis, BALB/c mice were less susceptible to anti-PD-1 treatment, as cardiac dysfunction and left ventricular dilation did not develop in this strain. Interestingly, compared with C57BL/6J mice, in the thymus, the anti-inflammatory cytokine *Il10* was up-regulated, leading to a more balanced IL-17/IL-10 ratio. This conclusion suggests that subtle differences in systemic immune response to PD-1 inhibition may predispose to cardiotoxicity development.

Accordingly, interventions targeting cytokine expression have prevented the development of PD-1 inhibition-induced cardiac dysfunction. While it has been shown previously that ICI-induced myocarditis is mediated mainly by CD8^{+} T-cells (Wei et al., 2020), and targeting this cell population can prevent the decrease in cardiac function (Michel et al., 2022) Here, we have shown that CD4^{+} T-cells also contribute to the development of anti-PD-1-induced cardiac dysfunction, likely through the production of various cytokines. In line with this hypothesis, specific targeting of IL-17A with a monoclonal antibody during anti-PD-1 treatment prevented the development of cardiac dysfunction. IL-17 blocking antibodies are currently in clinical use, for the treatment of psoriasis (Ghoreschi et al., 2021). Recently, blocking antibodies have been shown to be effective in alleviating ICI-induced immune-related adverse effects (irAEs) in some cases (Johnson et al., 2019; Lechner et al., 2022), whereas inhibition of

IL-17A improved the anti-tumour effect of ICI treatment in preclinical studies (Liu et al., 2021; Nagaoka et al., 2020). Taken together, pharmacological treatment aimed at IL-17A with currently available antibodies could be a clinically relevant adjuvant to immune checkpoint blockade, because it can alleviate ICI-mediated cardiotoxicity and other irAEs, while not interfering with, or even improving the anti-cancer effects.

To investigate the transcriptomic changes occurring in the heart after pharmacological PD-1 inhibition, we have performed analysis of the cardiac transcriptome of isotype control and anti-PD-1 treated C57BL/6J mice with bulk RNA sequencing. Immune checkpoint inhibition with anti-PD-1 treatment resulted in a distinct transcriptomic profile, with changes most prominently involving cardiac contractile processes and antigen presentation, as revealed by Gene Ontology Enrichment analysis of the differentially expressed genes. Of the differentially expressed genes, several have been previously associated with cardiac dysfunction and heart failure.

First, genes with roles in cardiac structure and function were assessed. The dystrophin gene (*Dmd*) was found to be down-regulated due to PD-1 inhibition in C57BL/6J mice, whereas it increased in BALB/c mice. Dystrophin is a key structural protein in muscle cells, linking the cytoskeleton and extracellular matrix and providing structural stability. Mutations in the *Dmd* gene are responsible for Duchenne and Becker muscular dystrophies, presenting with dilated cardiomyopathy among skeletal muscle-related and other symptoms (Kamdar & Garry, 2016). In preclinical studies, loss of dystrophin has been associated with contractile dysfunction and progression to heart failure in abdominal aorta banded mice (Prado et al., 2017), while decrease in dystrophin levels was observed in mice after myocardial infarction-induced heart failure (Yoshida et al., 2003). Furthermore, dystrophin-deficiency resulted in metabolic and signalling alterations in the heart before overt signs of heart failure appeared (Khairallah et al., 2007), suggesting that dystrophin is involved in various cardiac processes among structural stability of muscle cells. The expression of Lim domain binding 3 (*Ldb3*) showed a similar pattern. LDB3 plays a role in muscle cell structure, maintaining Z-line integrity during contraction (Weeland et al., 2015). Mutations in *Ldb3* have been implicated in dilated cardiomyopathy previously (Vatta et al., 2003). *Fxyd2*, encoding the γ subunit of Na$^+$-K$^+$-ATPase, increased prominently in C57BL/6J mice, butwas not affected in BALB/c mice. Although *Fxyd2* has been described to play a physiological role in the kidney (Kamdar & Garry, 2016), the marked increase seen in the hearts of mice with cardiac dysfunction suggests a potential role in cardiac function as well.

Signalling molecules *Stat3* and *Gsk3b* both decreased in C57BL/6J mice, while increased in BALB/c mice. Signal transducer and activator of transcription 3 (STAT3) has been implicated in a vital role for maintaining normal cardiac function under stress conditions (Kurdi et al., 2018). Cardiac knock-out of *Stat3* leads to decreased contractile function in mice with angiotensin II-induced hypertension, without exacerbating cardiac hypertrophy (Altara, Harmancey, et al., 2016). Interestingly, STAT3 has been shown to protect against the dilation phenotype in viral myocarditis by maintaining the

expression of dystrophin (Yajima et al., 2006). Glycogen synthase kinase 3β (GSK3β) activity has been shown to be decreased in heart failure (Haq et al., 2001). However, this is potentially a compensatory mechanism, since GSK3β inhibition has been shown to be cardioprotective in a pressure-overload induced mouse heart failure model (Hirotani et al., 2007).

Furthermore, the cardiac response to parasympathetic stimuli seems to be dysregulated as well, with the decreased expression of *Chrm2* in C57BL/6J mice and increase in BALB/c mice. *Chrm2* is responsible for M2 muscarinic acetylcholine receptor production. Deficiency of M2 muscarinic acetylcholine receptors has been shown to increase the susceptibility of the heart to the detrimental effects of chronic adrenergic stimulation (LaCroix et al., 2008), whereas a missense mutation in the gene has been associated with familial dilated cardiomyopathy (Zhang et al., 2008).

Transcriptomic changes in the myocardium related to inflammatory pathways were also found to be altered by anti-PD-1 treatment. *Cxcl9* was up-regulated in the hearts of C57BL/6J mice, which produces the pro-inflammatory chemokine (C-X-C motif) ligand 9 (CXCL9). CXCL9 is the ligand for **CXCR3** and induces chemotaxis and leukocyte extravasation. In patients with heart failure, circulating CXCL9 has been associated with disease severity (Altara, Mallat, et al., 2016). Furthermore, the CXCL9/**CXCL10**-CXCR3 axis have been implicated in the pathogenesis of heart failure. In mice, CXCR3 deficiency ameliorated the progression of pressure-overload induced heart failure, by inhibiting T-cell migration into the myocardium (Ngwenyama et al., 2019). In a clinical study, increased CXCL9 serum levels have been observed after ICI therapy. Of note, patients with irAEs exhibited greater increase in CXCL9 compared with patients without irAEs (Khan et al., 2019). *Nfkbia*, encoding IκBα, and inhibitor of NF-κB, was found to be down-regulated after 2 weeks of ICI therapy in C57BL/6J mice, while it increased in BALB/c mice. Degradation of IκBα and subsequent activation of NF-κB in septic mice have been shown to contribute to cardiac dysfunction (Li et al., 2014).

In our data set, *Ass1* was the most significantly up-regulated gene. Argininosuccinate synthetase, the product of *Ass1*, is the rate-limiting step in **arginine** production from citrulline, which is the substrate of NO synthases (Husson et al., 2003). *Ass1* was shown to be up-regulated by inflammatory cytokines, such as IL-1β (Flodström et al., 1995), while in LPS-treated rats, *Ass1* and *iNOS* were co-induced (Nagasaki et al., 1996).

Taken together, our results show that anti-PD-1 therapy leads to impaired cardiac function even without T-cell infiltration into the myocardium in C57BL/6J mice. ICI-induced cardiac dysfunction presents with a unique transcriptomic profile related to cardiac structure, signalling and inflammation, while nitrosative stress is increased in the heart. Beside local alterations in the myocardium, anti-PD-1 treatment leads to an enhanced systemic immune response, with increased pro-inflammatory cytokine expression seen most prominently in the thymus. Differences in systemic immune response to PD-1 inhibition may determine the susceptibility to cardiotoxicity, because BALB/c mice were resistant to the development of cardiac dysfunction. Targeting pro-inflammatory cytokine

expression non-specifically (by depleting CD4$^+$ T-cells) or by specific inhibition of IL-17A, prevented anti-PD-1-induced cardiac dysfunction. These findings provide insights about the underlying mechanisms of ICI-induced cardiac dysfunction and heart failure, whereas repurposing IL-17A blocking antibodies could be a potential pharmacological intervention to alleviate anti-PD-1-induced cardiotoxicity.

AUTHOR CONTRIBUTIONS

Tamás G. Gergely: Conceptualization (lead); data curation (lead); formal analysis (lead); investigation (lead); methodology (lead); visualization (lead); writing-original draft (lead); writing-review and editing (equal). **Dániel Kucsera:** Investigation (equal); methodology (equal); writing-review and editing (equal). **Viktória E Tóth:** Investigation (equal); methodology (equal); writing-review and editing (equal). **Tamás Kovács:** Investigation (equal); methodology (equal); writing-review and editing (equal). **Nabil Viktor Sayour:** Investigation (equal); methodology (equal); writing-review and editing (equal). **Zsófia D. Drobni:** Methodology (equal); writing-review and editing (equal). **Mihály Ruppert:** Investigation (equal); methodology (equal); writing-review and editing (equal). **Balázs Petrovich:** Data curation (equal); methodology (equal); software (lead); visualization (equal); writing-review and editing (equal). **Bence Ágg:** Data curation (equal); methodology (equal); software (equal); supervision (equal); visualization (equal); writing-review and editing (equal). **Zsófia Onódi:** Investigation (equal); methodology (equal); writing-review and editing (equal). **Nóra Fekete:** Investigation; methodology; writing-review and editing. **Éva Pállinger:** Investigation (equal); methodology (equal); supervision (equal); writing-review and editing (equal). **Edit I. Buzás:** Funding acquisition (equal); resources (equal); supervision (equal); writing-review and editing (equal). **Laura I. Yousif:** Investigation (equal); methodology (equal); writing-review and editing (equal). **Wouter C. Meijers:** Investigation (equal); methodology (equal); software (equal); supervision (equal); writing-review and editing (equal). **Tamás Radovits:** Funding acquisition (equal); supervision (equal); writing-review and editing (equal). **Béla Merkely:** Funding acquisition (equal); resources (equal); writing-review and editing (equal). **Péter Ferdinandy:** Funding acquisition (equal); methodology (equal); resources (equal); software (equal); supervision (equal); writing-review and editing (equal). **Zoltán V. Varga:** Conceptualization (lead); funding acquisition (lead); investigation (equal); methodology (lead); project administration (equal); resources (lead); supervision (lead); visualization (equal); writing-original draft (lead); writing-review and editing (lead).

CONFLICT OF INTEREST

On behalf of all authors, the corresponding author states that there is no conflict of interest. PF is the founder and CEO of Pharmahungary Group, a group of R&D companies.

DECLARATION OF TRANSPARENCY AND SCIENTIFIC RIGOUR

This Declaration acknowledges that this paper adheres to the principles for transparent reporting and scientific rigour of preclinical research as stated in the BJP guidelines for Natural Products Research, Design and Analysis, Immunoblotting and Immunochemistry, and Animal Experimentation, and as recommended by funding agencies, publishers and other organizations engaged with supporting research.

DATA AVAILABILITY STATEMENT

The data that support the findings of this study are available from the corresponding author upon reasonable request. Data from the RNA sequencing experiments are publicly available at ArrayExpress (https://www.ebi.ac.uk/biostudies/arrayexpress) under the accession number E-MTAB-12388.

ORCID

Tamás G. Gergely https://orcid.org/0000-0003-1972-2065
Bence Ágg https://orcid.org/0000-0002-6492-0426
Zsófia Onódi https://orcid.org/0000-0002-3746-8016
Zoltán V. Varga https://orcid.org/0000-0002-2758-0784

REFERENCES

Alexander, S. P. H., Christopoulos, A., Davenport, A. P., Kelly, E., Mathie, A., Peters, J. A., Veale, E. L., Armstrong, J. F., Faccenda, E., Harding, S. D., Pawson, A. J., Southan, C., Davies, J. A., Abbracchio, M. P., Alexander, W., Al-Hosaini, K., Bäck, M., Barnes, N. M., Bathgate, R., … Ye, R. D. (2021). The concise guide to pharmacology 2021/22: G protein-coupled receptors. *British Journal of Pharmacology*, *178*(S1), S27–S156. https://doi.org/10.1111/bph.15538

Alexander, S. P. H., Cidlowski, J. A., Kelly, E., Mathie, A., Peters, J. A., Veale, E. L., Armstrong, J. F., Faccenda, E., Harding, S. D., Pawson, A. J., Southan, C., Davies, J. A., Coons, L., Fuller, P. J., Korach, K. S., & Young, M. J. (2021). The concise guide to pharmacology 2021/22: Nuclear hormone receptors. *British Journal of Pharmacology*, *178*(S1), S246–S263. https://doi.org/10.1111/bph.15540

Alexander, S. P. H., Fabbro, D., Kelly, E., Mathie, A., Peters, J. A., Veale, E. L., Armstrong, J. F., Faccenda, E., Harding, S. D., Pawson, A. J., Southan, C., Davies, J. A., Annett, S., Boison, D., Burns, K. E., Dessauer, C., Gertsch, J., Helsby, N. A., Izzo, A. A., … Wong, S. S. (2021). The concise guide to pharmacology 2021/22: Enzymes. *British Journal of Pharmacology*, *178*(S1), S313–S411. https://doi.org/10.1111/bph.15542

Alexander, S. P. H., Fabbro, D., Kelly, E., Mathie, A., Peters, J. A., Veale, E. L., Armstrong, J. F., Faccenda, E., Harding, S. D., Pawson, A. J., Southan, C., Davies, J. A., Beuve, A., Brouckaert, P., Bryant, C., Burnett, J. C., Farndale, R. W., Friebe, A., Garthwaite, J., … Waldman, S. A. (2021). The concise guide to pharmacology 2021/22: Catalytic receptors. *British Journal of Pharmacology*, *178*(S1), S264–S312. https://doi.org/10.1111/bph.15541

Alexander, S. P. H., Kelly, E., Mathie, A., Peters, J. A., Veale, E. L., Armstrong, J. F., Faccenda, E., Harding, S. D., Pawson, A. J., Southan, C., Buneman, O. P., Cidlowski, J. A., Christopoulos, A., Davenport, A. P., Fabbro, D., Spedding, M., Striessnig, J., Davies, J. A., Ahlers-Dannen, K. E., … Zolghadri, Y. (2021). The concise guide to pharmacology 2021/22: Introduction and other protein targets. *British Journal of Pharmacology*, *178*(S1), S1–S26. https://doi.org/10.1111/bph.15537

Alexander, S. P. H., Kelly, E., Mathie, A., Peters, J. A., Veale, E. L., Armstrong, J. F., Faccenda, E., Harding, S. D., Pawson, A. J., Southan, C., Davies, J. A., Amarosi, L., Anderson, C. M. H., Beart, P. M., Broer, S., Dawson, P. A., Hagenbuch, B., Hammond, J. R., Hancox, J. C., ... Verri, T. (2021). The concise guide to pharmacology 2021/22: Transporters. British Journal of Pharmacology, 178(S1), S412–S513. https://doi.org/10.1111/bph.15543

Alexander, S. P. H., Mathie, A., Peters, J. A., Veale, E. L., Striessnig, J., Kelly, E., Armstrong, J. F., Faccenda, E., Harding, S. D., Pawson, A. J., Southan, C., Davies, J. A., Aldrich, R. W., Attali, B., Baggetta, A. M., Becirovic, E., Biel, M., Bill, R. M., Catterall, W. A., ... Zhu, M. (2021). The concise guide to pharmacology 2021/22: Ion channels. British Journal of Pharmacology, 178(S1), S157–S245. https://doi.org/10.1111/bph.15539

Altara, R., Harmancey, R., Didion, S. P., Booz, G. W., & Zouein, F. A. (2016). Cardiac STAT3 deficiency impairs contractility and metabolic homeostasis in hypertension. Frontiers in Pharmacology, 7(NOV), 1–8. https://doi.org/10.3389/fphar.2016.00436

Altara, R., Mallat, Z., Booz, G. W., & Zouein, F. A. (2016). The CXCL10/CXCR3 axis and cardiac inflammation: Implications for immunotherapy to treat infectious and noninfectious diseases of the heart. Journal of Immunology Research, 2016, 1–12, 4396368. https://doi.org/10.1155/2016/4396368

Anderson, R. D., & Brooks, M. (2016). Apical takotsubo syndrome in a patient with metastatic breast carcinoma on novel immunotherapy. International Journal of Cardiology, 222, 760–761. https://doi.org/10.1016/j.ijcard.2016.07.291

Baldeviano, G. C., Barin, J. G., Talor, M. V., Srinivasan, S., Bedja, D., Zheng, D., Gabrielson, K., Iwakura, Y., Rose, N. R., & Cihakova, D. (2010). Interleukin-17A is dispensable for myocarditis but essential for the progression to dilated cardiomyopathy. Circulation Research, 106(10), 1646–1655. https://doi.org/10.1161/CIRCRESAHA.109.213157

Benjamini, Y., & Hochberg, Y. (1995). Controlling the false discovery rate: A practical and powerful approach to multiple testing. Journal of the Royal Statistical Society, Series B, 57(1), 289–300. [Online]. http://www.stat.purdue.edu/~doerge/BIOINFORM.D/FALL06/Benjamini%26and%26Y%26FDR.pdf%5Cn; http://engr.case.edu/ray_soumya/mlrg/controlling_fdr_benjamini95.pdf

Curtis, M. J., Alexander, S., Cirino, G., Docherty, J. R., George, C. H., Giembycz, M. A., Hoyer, D., Insel, P. A., Izzo, A. A., Ji, Y., MacEwan, D. J., Sobey, C. G., Stanford, S. C., Teixeira, M. M., Wonnacott, S., & Ahluwalia, A. (2018). Experimental design and analysis and their reporting II: Updated and simplified guidance for authors and peer reviewers. British Journal of Pharmacology, 175(7), 987–993. https://doi.org/10.1111/bph.14153

D'Souza, M., Nielsen, D., Svane, I. M., Iversen, K., Rasmussen, P. V., Madelaire, C., Fosbøl, E., Køber, L., Gustafsson, F., Andersson, C., Gislason, G., Torp-Pedersen, C., & Schou, M. (2020). The risk of cardiac events in patients receiving immune checkpoint inhibitors: A nationwide Danish study. European Heart Journal, 42, 1621–1631. https://doi.org/10.1093/eurheartj/ehaa884

Devereux, R. B., Alonso, D. R., Lutas, E. M., Gottlieb, G. J., Campo, E., Sachs, I., & Reichek, N. (1986). Echocardiographic assessment of left ventricular hypertrophy: Comparison to necropsy findings. The American Journal of Cardiology, 57(6), 450–458. https://doi.org/10.1016/0002-9149(86)90771-X

Dolladille, C., Ederhy, S., Allouche, S., Dupas, Q., Gervais, R., Madelaine, J., Sassier, M., Plane, A. F., Comoz, F., Cohen, A. A., Thuny, F. R., Cautela, J., & Alexandre, J. (2020). Late cardiac adverse events in patients with cancer treated with immune checkpoint inhibitors. Journal for Immunotherapy of Cancer, 8(1), 1–10. https://doi.org/10.1136/jitc-2019-000261

Drobni, Z. D., Alvi, R. M., Taron, J., Zafar, A., Murphy, S. P., Rambarat, P. K., Mosarla, R. C., Lee, C., Zlotoff, D. A., Raghu, V. K., Hartmann, S. E.,

Gilman, H. K., Gong, J., Zubiri, L., Sullivan, R. J., Reynolds, K. L., Mayrhofer, T., Zhang, L., Hoffmann, U., & Neilan, T. G. (2020). Association between immune checkpoint inhibitors with cardiovascular events and atherosclerotic plaque. Circulation, 142, 2299–2311. https://doi.org/10.1161/CIRCULATIONAHA.120.049981

Dulos, J., Carven, G. J., van Boxtel, S. J., Evers, S., Driessen-Engels, L. J. A., Hobo, W., Gorecka, M. A., de Haan, A. F. J., Mulders, P., Punt, C. J. A., Jacobs, J. F. M., Schalken, J. A., Oosterwijk, E., van Eenennaam, H., & Boots, A. M. (2012). PD-1 blockade augments Th1 and Th17 and suppresses Th2 responses in peripheral blood from patients with prostate and advanced melanoma cancer. Journal of Immunotherapy, 35(2), 169–178. https://doi.org/10.1097/CJI.0b013e318247a4e7

Ederhy, S., Cautela, J., Ancedy, Y., Escudier, M., Thuny, F., & Cohen, A. (2018). Takotsubo-like syndrome in cancer patients treated with immune checkpoint inhibitors. JACC: Cardiovascular Imaging, 11(8), 1187–1190. https://doi.org/10.1016/j.jcmg.2017.11.036

Escudier, M., Cautela, J., Malissen, N., Ancedy, Y., Orabona, M., Pinto, J., Monestier, S., Grob, J. J., Scemama, U., Jacquier, A., Lalevee, N., Barraud, J., Peyrol, M., Laine, M., Bonello, L., Paganelli, F., Cohen, A., Barlesi, F., Ederhy, S., & Thuny, F. (2017). Clinical features, management, and outcomes of immune checkpoint inhibitor-related cardiotoxicity. Circulation, 136(21), 2085–2087. https://doi.org/10.1161/CIRCULATIONAHA.117.030571

Ewels, P., Magnusson, M., Lundin, S., & Käller, M. (2016). MultiQC: Summarize analysis results for multiple tools and samples in a single report. Bioinformatics, 32(19), 3047–3048. https://doi.org/10.1093/bioinformatics/btw354

Ferdinandy, P., Danial, H., Ambrus, I., Rothery, R. A., & Schulz, R. (2000). Peroxynitrite is a major contributor to cytokine-induced myocardial contractile failure. Circulation Research, 87(3), 241–247. https://doi.org/10.1161/01.RES.87.3.241

Flodström, M., Niemann, A., Bedoya, F. J., Morris, S. M., & Eizirik, D. L. (1995). Expression of the citrulline-nitric oxide cycle in rodent and human pancreatic beta-cells: Induction of argininosuccinate synthetase by cytokines. Endocrinology, 136(8), 3200–3206. https://doi.org/10.1210/endo.136.8.7628352

Gedye, C., van der Westhuizen, A., & John, T. (2015). Checkpoint immunotherapy for cancer: Superior survival, unaccustomed toxicities. Internal Medicine Journal, 45(7), 696–701. https://doi.org/10.1111/imj.12653

Geisler, B. P., Raad, R. A., Esaian, D., Sharon, E., & Schwartz, D. R. (2015). Apical ballooning and cardiomyopathy in a melanoma patient treated with ipilimumab: A case of takotsubo-like syndrome. Journal for Immunotherapy of Cancer, 3(1), 4–7. https://doi.org/10.1186/s40425-015-0048-2

Ghoreschi, K., Balato, A., Enerbäck, C., & Sabat, R. (2021). Therapeutics therapeutics targeting the IL-23 and IL-17 pathway in psoriasis. Lancet, 397(10275), 754–766. https://doi.org/10.1016/S0140-6736(21)00184-7

Haq, S., Choukroun, G., Lim, H., Tymitz, K. M., del Monte, F., Gwathmey, J., Grazette, L., Michael, A., Hajjar, R., Force, T., & Molkentin, J. D. (2001). Differential activation of signal transduction pathways in human hearts with hypertrophy versus advanced heart failure. Circulation, 103(5), 670–677. https://doi.org/10.1161/01.CIR.103.5.670

Heinzerling, L., Ott, P. A., Hodi, F. S., Husain, A. N., Tajmir-Riahi, A., Tawbi, H., Pauschinger, M., Gajewski, T. F., Lipson, E. J., & Luke, J. J. (2016). Cardiotoxicity associated with CTLA4 and PD1 blocking immunotherapy. Journal for Immunotherapy of Cancer, 4(1), 50. https://doi.org/10.1186/s40425-016-0152-y

Hirotani, S., Zhai, P., Tomita, H., Galeotti, J., Marquez, J. P., Gao, S., Hong, C., Yatani, A., Avila, J:., & Sadoshima, J. (2007). Inhibition of glycogen synthase kinase 3β during heart failure is protective. Circulation Research, 101(11), 1164–1174. https://doi.org/10.1161/CIRCRESAHA.107.160614

Hu, J.-R., Florido, R., Lipson, E. J., Naidoo, J., Ardehali, R., Tocchetti, C. G., Lyon, A. R., Padera, R. F., Johnson, D. B., & Moslehi, J. (2019).

Cardiovascular toxicities associated with immune checkpoint inhibitors. *Cardiovascular Research*, 115, 854–868. https://doi.org/10.1093/cvr/cvz026

Husson, A., Brasse-Lagnel, C., Fairand, A., Renouf, S., & Lavoinne, A. (2003). Argininosuccinate synthetase from the urea cycle to the citrulline-NO cycle. *European Journal of Biochemistry*, 270(9), 1887–1899. https://doi.org/10.1046/j.1432-1033.2003.03559.x

Izzo, A. A., Teixeira, M., Alexander, S. P., Cirino, G., Docherty, J. R., George, C. H., Insel, P. A., Ji, Y., Kendall, D. A., Panattieri, R. A., Sobey, C. G., Stanford, S. C., Stefanska, B., Stephens, G., & Ahluwalia, A. (2020). A practical guide for transparent reporting of research on natural products in the *British Journal of Pharmacology*: Reproducibility of natural product research. *British Journal of Pharmacology*, 177(10), 2169–2178. https://doi.org/10.1111/bph.15054

Johnson, D., Patel, A. B., Uemura, M. I., Trinh, V. A., Jackson, N., Zobniw, C. M., Tetzlaff, M. T., Hwu, P., Curry, J. L., & Diab, A. (2019). IL17A blockade successfully treated Psoriasiform dermatologic toxicity from immunotherapy. *Cancer Immunology Research*, 7(June), 860–865. https://doi.org/10.1158/2326-6066.CIR-18-0682

Johnson, D. B., Balko, J. M., Compton, M. L., Chalkias, S., Gorham, J., Xu, Y., Hicks, M., Puzanov, I., Alexander, M. R., Bloomer, T. L., Becker, J. R., Slosky, D. A., Phillips, E. J., Pilkinton, M. A., Craig-Owens, L., Kola, N., Plautz, G., Reshef, D. S., Deutsch, J. S., … Moslehi, J. J. (2016). Fulminant myocarditis with combination immune checkpoint blockade. *The New England Journal of Medicine*, 375(18), 1749–1755. https://doi.org/10.1056/NEJMoa1609214

Kamdar, F., & Garry, D. J. (2016). Dystrophin-deficient cardiomyopathy. *Journal of the American College of Cardiology*, 67(21), 2533–2546. https://doi.org/10.1016/j.jacc.2016.02.081

Khairallah, M., Khairallah, R., Young, M. E., Dyck, J. R. B., Petrof, B. J., & Des Rosiers, C. (2007). Metabolic and signaling alterations in dystrophin-deficient hearts precede overt cardiomyopathy. *Journal of Molecular and Cellular Cardiology*, 43(2), 119–129. https://doi.org/10.1016/j.yjmcc.2007.05.015

Khan, S., Khan, S. A., Luo, X., Fattah, F. J., Saltarski, J., Gloria-McCutchen, Y., Lu, R., Xie, Y., Li, Q., Wakeland, E., & Gerber, D. E. (2019). Immune dysregulation in cancer patients developing immune-related adverse events. *British Journal of Cancer*, 120(1), 63–68. https://doi.org/10.1038/s41416-018-0155-1

Kim, D., Paggi, J. M., Park, C., Bennett, C., & Salzberg, S. L. (2019). Graph-based genome alignment and genotyping with HISAT2 and HISAT-genotype. *Nature Biotechnology*, 37(8), 907–915. https://doi.org/10.1038/s41587-019-0201-4

Konstantina, T., Konstantinos, R., Anastasios, K., Anastasia, M., Eleni, L., Ioannis, S., Sofia, A., & Dimitris, M. (2019). Fatal adverse events in two thymoma patients treated with anti-PD-1 immune check point inhibitor and literature review. *Lung Cancer*, 135(April), 29–32. https://doi.org/10.1016/j.lungcan.2019.06.015

Kurdi, M., Zgheib, C., & Booz, G. W. (2018). Recent developments on the crosstalk between STAT3 and inflammation in heart function and disease. *Frontiers in Immunology*, 9(December), 1–10. https://doi.org/10.3389/fimmu.2018.03029

LaCroix, C., Freeling, J., Giles, A., Wess, J., & Li, Y. F. (2008). Deficiency of M2 muscarinic acetylcholine receptors increases susceptibility of ventricular function to chronic adrenergic stress. *American Journal of Physiology: Heart and Circulatory Physiology*, 294(2), 810–820. https://doi.org/10.1152/ajpheart.00724.2007

Lechner, M. G., Cheng, M. I., Patel, A. Y., Hoang, A. T., Yakobian, N., Astourian, M., Pioso, M. S., Rodriguez, E. D., McCarthy, E. C., Hugo, W., Angell, T. E., Drakaki, A., Ribas, A., & Su, M. A. (2022). Inhibition of IL-17A protects against thyroid immune-related adverse events while preserving checkpoint inhibitor antitumor efficacy. *Journal of*

Immunology, 209, 696–709. https://doi.org/10.4049/jimmunol.2200244

Li, X., Luo, R., Chen, R., Song, L., Zhang, S., Hua, W., & Chen, H. (2014). Cleavage of IκBα by calpain induces myocardial NF-κB activation, TNF-α expression, and cardiac dysfunction in septic mice. *American Journal of Physiology. Heart and Circulatory Physiology*, 306(6), 833–843. https://doi.org/10.1152/ajpheart.00893.2012

Liao, Y., Smyth, G. K., & Shi, W. (2014). FeatureCounts: An efficient general purpose program for assigning sequence reads to genomic features. *Bioinformatics*, 30(7), 923–930. https://doi.org/10.1093/bioinformatics/btt656

Lilley, E., Stanford, S. C., Kendall, D. E., Alexander, S. P., Cirino, G., Docherty, J. R., George, C. H., Insel, P. A., Izzo, A. A., Ji, Y., Panattieri, R. A., Sobey, C. G., Stefanska, B., Stephens, G., Teixeira, M., & Ahluwalia, A. (2020). ARRIVE 2.0 and the *British Journal of Pharmacology*: Updated guidance for 2020. *British Journal of Pharmacology*, 177(16), 3611-3616. https://bpspubs.onlinelibrary.wiley.com/doi/full/10.1111/bph.15178

Liu, C., Liu, R., Wang, B., Lian, J., Yao, Y., Sun, H., Zhang, C., Fang, L., Guan, X., Shi, J., Han, S., Zhan, F., Luo, S., Yao, Y., Zheng, T., & Zhang, Y. (2021). Blocking IL-17A enhances tumor response to anti-PD-1 immunotherapy in microsatellite stable colorectal cancer. *Journal for Immunotherapy of Cancer*, 9(1), e001895. https://doi.org/10.1136/jitc-2020-001895

Love, M. I., Huber, W., & Anders, S. (2014). Moderated estimation of fold change and dispersion for RNA-seq data with DESeq2. *Genome Biology*, 15(12), 1–21. https://doi.org/10.1186/s13059-014-0550-8

Mahmood, S. S., Fradley, M. G., Cohen, J. V., Nohria, A., Reynolds, K. L., Heinzerling, L. M., Sullivan, R. J., Damrongwatanasuk, R., Chen, C. L., Gupta, D., Kirchberger, M. C., Awadalla, M., Hassan, M. Z. O., Moslehi, J. J., Shah, S. P., Ganatra, S., Thavendiranathan, P., Lawrence, D. P., Groarke, J. D., & Neilan, T. G. (2018). Myocarditis in patients treated with immune checkpoint inhibitors. *Journal of the American College of Cardiology*, 71(16), 1755–1764. https://doi.org/10.1016/j.jacc.2018.02.037

Martin, M. (2011). Cutadapt removes adapter sequences from high-throughput sequencing reads. *EMBnet.Journal*, 17, 10–12. https://doi.org/10.14806/ej.17.1.200

Mencel, J., Gargett, T., Karanth, N., Pokorny, A., Brown, M. P., & Charakidis, M. (2019). Thymic hyperplasia following double immune checkpoint inhibitor therapy in two patients with stage IV melanoma. *Asia-Pacific Journal of Clinical Oncology*, 15(6), 383–386. https://doi.org/10.1111/ajco.13233

Mi, H., Muruganujan, A., Ebert, D., Huang, X., & Thomas, P. D. (2019). PANTHER version 14: More genomes, a new PANTHER GO-slim and improvements in enrichment analysis tools. *Nucleic Acids Research*, 47(D1), D419–D426. https://doi.org/10.1093/nar/gky1038

Michel, L., Helfrich, I., Hendgen-Cotta, U. B., Mincu, R. I., Korste, S., Mrotzek, S. M., Spomer, A., Odersky, A., Rischpler, C., Herrmann, K., Umutlu, L., Coman, C., Ahrends, R., Sickmann, A., Löffek, S., Livingstone, E., Ugurel, S., Zimmer, L., Gunzer, M., … Rassaf, T. (2022). Targeting early stages of cardiotoxicity from anti-PD1 immune checkpoint inhibitor therapy. *European Heart Journal*, 43(4), 316–329. https://doi.org/10.1093/eurheartj/ehab430

Myers, J. M., Cooper, L. T., Kem, D. C., Stavrakis, S., Kosanke, S. D., Shevach, E. M., Fairweather, D., Stoner, J. A., Cox, C. J., & Cunningham, M. W. (2016). Cardiac myosin-Th17 responses promote heart failure in human myocarditis. *JCI Insight*, 1(9), e85851. https://doi.org/10.1172/jci.insight.85851

Nagaoka, K., Shirai, M., Taniguchi, K., Hosoi, A., Sun, C., Kobayashi, Y., Maejima, K., Fujita, M., Nakagawa, H., Nomura, S., & Kakimi, K. (2020). Deep immunophenotyping at the cell level identifies a combination of anti-IL-17 and checkpoint blockade as an effective treatment in a

preclinical model of data-guided personalized immunotherapy. *Journal for Immunotherapy of Cancer*, 8, 1–14. https://doi.org/10.1136/jitc-2020-001358

Nagasaki, A., Gotoh, T., Takeya, M., Yu, Y., Takiguchi, M., Matsuzaki, H., Takatsuki, K., & Mori, M. (1996). Coinduction of nitric oxide synthase, argininosuccinate synthetase, and argininosuccinate lyase in lipopolysaccharide-treated rats: RNA blot, immunoblot, and immunohistochemical analyses. *The Journal of Biological Chemistry*, 271(5), 2658–2662. https://doi.org/10.1074/jbc.271.5.2658

Ngwenyama, N., Salvador, A. M., Velázquez, F., Nevers, T., Levy, A., Aronovitz, M., Luster, A. D., Huggins, G. S., & Alcaide, P. (2019). CXCR3 regulates CD4$^+$ T cell cardiotropism in pressure overload–induced cardiac dysfunction. *JCI Insight*, 4(7), e125527. https://doi.org/10.1172/jci.insight.125527

Nishimura, H., Okazaki, T., Tanaka, Y., Nakatani, K., Hara, M., Matsumori, A., Sasayama, S., Mizoguchi, A., Hiai, H., Minato, N., & Honjo, T. (2001). Autoimmune dilated cardiomyopathy in PD-1 receptor-deficient mice. *Science (80-.)*, 291(5502), 319–322. https://doi.org/10.1126/science.291.5502.319

Pacher, P., Schulz, R., Liaudet, L., & Szabó, C. (2005). Nitrosative stress and pharmacological modulation of heart failure. *Trends in Pharmacological Sciences*, 26(6), 302–310. https://doi.org/10.1016/j.tips.2005.04.003

Percie du Sert, N., Hurst, V., Ahluwalia, A., Alam, S., Avey, M. T., Baker, M., Browne, W. J., Clark, A., Cuthill, I. C., Dirnagl, U., Emerson, M., Garner, P., Holgate, S. T., Howells, D. W., Karp, N. A., Lazic, S. E., Lidster, K., MacCallum, C., Macleod, M., … Würbel, H. (2020). The arrive guidelines 2.0: Updated guidelines for reporting animal research. *PLoS Biology*, 18(7), 1–12. https://doi.org/10.1371/journal.pbio.3000410

Postow, M. A., Sidlow, R., & Hellmann, M. D. (2018). Immune-related adverse events associated with immune checkpoint blockade. *The New England Journal of Medicine*, 378(2), 158–168. https://doi.org/10.1056/NEJMra1703481

Prado, F. P., dos Santos, D. O., Blefari, V., Silva, C. A., Machado, J., Kettelhut, I. C., Ramos, S. G., Baruffi, M. D., Salgado, H. C., & Prado, C. M. (2017). Early dystrophin loss is coincident with the transition of compensated cardiac hypertrophy to heart failure. *PLoS ONE*, 12(12), 1–16. https://doi.org/10.1371/journal.pone.0189469

Roth, M. E., Muluneh, B., Jensen, B. C., Madamanchi, C., & Lee, C. B. (2016). Left ventricular dysfunction after treatment with ipilimumab for metastatic melanoma. *American Journal of Therapeutics*, 23(6), e1925–e1928. https://doi.org/10.1097/MJT.0000000000000430

Tarhini, A. A., Zahoor, H., Lin, Y., Malhotra, U., Sander, C., Butterfield, L. H., & Kirkwood, J. M. (2015). Baseline circulating IL-17 predicts toxicity while TGF-β1 and IL-10 are prognostic of relapse in ipilimumab neoadjuvant therapy of melanoma. *Journal for Immunotherapy of Cancer*, 3(1), 15–20. https://doi.org/10.1186/s40425-015-0081-1

Tay, W. T., Fang, Y. H., Beh, S. T., Liu, Y. W., Hsu, L. W., Yen, C. J., & Liu, P. Y. (2020). Programmed cell death-1: Programmed cell death-ligand 1 interaction protects human cardiomyocytes against T-cell mediated inflammation and apoptosis response in vitro. *International Journal of Molecular Sciences*, 21(7), 2399. https://doi.org/10.3390/ijms21072399

Vatta, M., Mohapatra, B., Jimenez, S., Sanchez, X., Faulkner, G., Perles, Z., Sinagra, G., Lin, J. H., Vu, T. M., Zhou, Q., Bowles, K. R., di Lenarda, A., Schimmenti, L., Fox, M., Chrisco, M. A., Murphy, R. T., McKenna, W., Elliott, P., Bowles, N. E., … Towbin, J. A. (2003). Mutations in cypher/ZASP in patients with dilated cardiomyopathy and left ventricular non-compaction. *Journal of the American College of Cardiology*, 42(11), 2014–2027. https://doi.org/10.1016/j.jacc.2003.10.021

von Euw, E., Chodon, T., Attar, N., Jalil, J., Koya, R. C., Comin-Anduix, B., & Ribas, A. (2009). CTLA4 blockade increases Th17 cells in patients with metastatic melanoma. *Journal of Translational Medicine*, 7, 1–13, 35. https://doi.org/10.1186/1479-5876-7-35

Watanabe, H., Numata, K., Ito, T., Takagi, K., & Matsukawa, A. (2004). Innate immune response in Th1- and Th2-dominant mouse strains. *Shock*, 22(5), 460–466. https://doi.org/10.1097/01.shk.0000142249.08135.e9

Weber, J., Mandala, M., del Vecchio, M., Gogas, H. J., Arance, A. M., Cowey, C. L., Dalle, S., Schenker, M., Chiarion-Sileni, V., Marquez-Rodas, I., Grob, J. J., Butler, M. O., Middleton, M. R., Maio, M., Atkinson, V., Queirolo, P., Gonzalez, R., Kudchadkar, R. R., Smylie, M., … Ascierto, P. A. (2017). Adjuvant nivolumab versus Ipilimumab in resected stage III or IV melanoma. *The New England Journal of Medicine*, 377(19), 1824–1835. https://doi.org/10.1056/nejmoa1709030

Weeland, C. J., van den Hoogenhof, M. M., Beqqali, A., & Creemers, E. E. (2015). Insights into alternative splicing of sarcomeric genes in the heart. *Journal of Molecular and Cellular Cardiology*, 81, 107–113. https://doi.org/10.1016/j.yjmcc.2015.02.008

Wei, S. C., Meijers, W. C., Axelrod, M. L., Anang, N. A. S., Screever, E. M., Wescott, E. C., Johnson, D. B., Whitley, E., Lehmann, L., Courand, P. Y., Mancuso, J. J., Himmel, L. E., Lebrun-Vignes, B., Wleklinski, M. J., Knollmann, B. C., Srinivasan, J., Li, Y., Atolagbe, O. T., Rao, X., … Allison, J. P. (2020). A genetic mouse model recapitulates immune checkpoint inhibitor-associated myocarditis and supports a mechanism-based therapeutic intervention. *Cancer Discovery*, 11, 614–625. https://doi.org/10.1158/2159-8290.CD-20-0856

Xue, G., Li, D. S., Wang, Z. Y., Liu, Y., Yang, J. M., Li, C. Z., Li, X. D., Ma, J. D., Zhang, M. M., Lu, Y. J., Li, Y., Yang, B. F., & Pan, Z. W. (2021). Interleukin-17 upregulation participates in the pathogenesis of heart failure in mice via NF-κB-dependent suppression of SERCA2a and Cav1.2 expression. *Acta Pharmacologica Sinica*, 42(February), 1780–1789. https://doi.org/10.1038/s41401-020-00580-6

Yajima, T., Yasukawa, H., Jeon, E. S., Xiong, D., Dorner, A., Iwatate, M., Nara, M., Zhou, H., Summers-Torres, D., Hoshijima, M., Chien, K. R., Yoshimura, A., & Knowlton, K. U. (2006). Innate defense mechanism against virus infection within the cardiac myocyte requiring gp130-STAT3 signaling. *Circulation*, 114(22), 2364–2373. https://doi.org/10.1161/CIRCULATIONAHA.106.642454

Yates, A., Akanni, W., Amode, M. R., Barrell, D., Billis, K., Carvalho-Silva, D., Cummins, C., Clapham, P., Fitzgerald, S., Gil, L., Girón, C. G., Gordon, L., Hourlier, T., Hunt, S. E., Janacek, S. H., Johnson, N., Juettemann, T., Keenan, S., Lavidas, I., … Flicek, P. (2016). Ensembl 2016. *Nucleic Acids Research*, 44(D1), D710–D716. https://doi.org/10.1093/nar/gkv1157

Yoshida, H., Takahashi, M., Koshimizu, M., Tanonaka, K., Oikawa, R., Toyo-oka, T., & Takeo, S. (2003). Decrease in sarcoglycans and dystrophin in failing heart following acute myocardial infarction. *Cardiovascular Research*, 59(2), 419–427. https://doi.org/10.1016/S0008-6363(03)00385-7

Zacchigna, S., Paldino, A., Falcão-Pires, I., Daskalopoulos, E. P., Dal Ferro, M., Vodret, S., Lesizza, P., Cannatà, A., Miranda-Silva, D., Lourenço, A. P., Pinamonti, B., Sinagra, G., Weinberger, F., Eschenhagen, T., Carrier, L., Kehat, I., Tocchetti, C. G., Russo, M., Ghigo, A., … Thum, T. (2021). Towards standardization of echocardiography for the evaluation of left ventricular function in adult rodents: A position paper of the ESC working group on myocardial function. *Cardiovascular Research*, 117(1), 43–59. https://doi.org/10.1093/cvr/cvaa110

Zaha, V. G., Meijers, W. C., & Moslehi, J. (2020). Cardio-Immuno-oncology. *Circulation*, *141*, 87–89. https://doi.org/10.1161/CIRCULATIONAHA.119.042276

Zhang, L., Hu, A., Yuan, H., Cui, L., Miao, G., Yang, X., Wang, L., Liu, J., Liu, X., Wang, S., Zhang, Z., Liu, L., Zhao, R., & Shen, Y. (2008). A missense mutation in the CHRM2 gene is associated with familial dilated cardiomyopathy. *Circulation Research*, *102*(11), 1426–1432. https://doi.org/10.1161/CIRCRESAHA.107.167783

SUPPORTING INFORMATION

Additional supporting information can be found online in the Supporting Information section at the end of this article.